High-Definition Hurricanes

Improving Forecasts with Storm-Following Nests

Ghassan J. Alaka Jr., Xuejin Zhang, and Sundararaman G. Gopalakrishnan

ABSTRACT: To forecast tropical cyclone (TC) intensity and structure changes with fidelity, numerical weather prediction models must be "high definition," i.e., horizontal grid spacing ≤ 3 km, so that they permit clouds and convection and resolve sharp gradients of momentum and moisture in the eyewall and rainbands. Storm-following nests are computationally efficient at fine resolutions, providing a practical approach to improve TC intensity forecasts. Under the Hurricane Forecast Improvement Project, the operational Hurricane Weather Research and Forecasting (HWRF) system was developed to include telescopic, storm-following nests for a single TC per model integration. Subsequently, HWRF evolved into a state-of-the-art tool for TC predictions around the globe, although its single-storm nesting approach does not adequately simulate TC–TC interactions as they are observed. Basin-scale HWRF (HWRF-B) was developed later with a multistorm nesting approach to improve the simulation of TC–TC interactions by producing high-resolution forecasts for multiple TCs simultaneously. In this study, the multistorm nesting approach in HWRF-B was compared with a single-storm nesting approach using an otherwise identical model configuration. The multistorm approach demonstrated TC intensity forecast improvements, including more realistic TC–TC interactions. Storm-following nests developed in HWRF and HWRF-B will be foundational to NOAA's next-generation hurricane application in the Unified Forecast System.

KEYWORDS: Hurricanes/typhoons; Tropical cyclones; Numerical weather prediction/forecasting; Model evaluation/performance; Forecast verification/skill

AFFILIATIONS: **Alaka, Zhang, and Gopalakrishnan**—NOAA/AOML/Hurricane Research Division, Miami, Florida

Tropical cyclone (TC) forecasts have improved dramatically over the last few decades, in part due to finer resolutions in numerical weather prediction (NWP) models. TC intensity and structure predictions require "high-definition" horizontal spatial scales (≤3 km) that are cloud permitting to adequately simulate the eyewall, rainbands, and sharp gradients of momentum and moisture therein. Although operational NWP models would be optimally configured with subkilometer horizontal grid spacing to explicitly resolve clouds, convection, and large eddies, that is simply not practical given today's computing power. Currently, operational, global NWP models have resolutions that are too coarse (≥9 km) to permit the simulation of clouds and other important small-scale processes in TCs. Outermost (i.e., "parent") domains in regional NWP models are also not operationally configured at cloud-permitting resolutions. Nested grids (i.e., "nests"), developed half a century ago (Hill 1968; Harrison and Elsberry 1972; Phillips and Shukla 1973), represent a solution to this operational inadequacy because they may be configured at fine (e.g., cloud-permitting) resolutions to simulate areas of interest, including TCs. Furthermore, nests are versatile in that they may be configured within global and regional domains, and nests may be placed within nests, creating a telescopic effect to achieve high-definition horizontal resolutions.

TCs often span multiple spatial scales, including the synoptic scale (e.g., the entire system), mesoscale (e.g., rainbands), misoscale (e.g., vortices within the eyewall), and microscale (e.g., turbulence in the inner core region). The ability to capture multiple spatial scales and the communication between those scales is a necessity for accurate TC intensity and structure predictions (Marks et al. 1998). High-definition nests receive information from the lower-resolution parent domain at the nest boundaries, and nests are allowed to communicate with the parent domain, creating a seamless flow of information between various scales of motion via what is commonly referred to as "two-way" interaction (Phillips and Shukla 1973; Zhang et al. 1986). As a result, larger spatial scales respond to smaller spatial scales in an NWP model simulation and vice versa, and this communication is vital for the production of accurate TC forecasts (Ley and Elsberry 1976; Kurihara and Bender 1980; Wang 2001; Gao et al. 2019).

Many TC research studies have used NWP models configured with nests that did not move during the model integration (e.g., Harrison 1973; Mathur 1974; Ookochi 1974; Wu et al. 2006; Rotunno et al. 2009; Lin et al. 2010; Hazelton et al. 2021). However, static nests large enough to contain a TC throughout a multiday forecast and that have resolution fine enough to realistically predict TC intensity and structure are computationally expensive and are not currently supported in operations. For example, Hazelton et al. (2021) highlighted a global-nested model configured with a high-resolution static nest that spanned the entire North Atlantic hurricane basin, and, while this approach yielded promising results, it is currently too expensive for operations. Furthermore, if static nests are too small, the TC could exit the high-resolution region, where intensity forecasts degrade significantly (Gopalakrishnan et al. 2006).

Moving nests (also known as "storm-following" nests) are more practical for TCs than static nests because they ensure that a feature of interest, such as a TC, is simulated at a resolution finer than what is provided by the parent domain throughout an entire forecast period (Harrison 1973; Ley and Elsberry 1976; Jones 1977; Kurihara et al. 1979). Moving nests were successfully implemented into the Fifth-generation Pennsylvania State University–National

Center for Atmospheric Research Mesoscale Model (MM5; Grell et al. 1995) for research applications (Liu et al. 1997; Kwon et al. 2002; Cangialosi et al. 2005). The infrastructure for moving nests was later incorporated into the WRF software architecture (Michalakes et al. 2005; Skamarock and Klemp 2008), marking the beginning of a new era for moving nests in a state-of-the-art NWP model for research. The Advanced Hurricane WRF (AHW) Model is one research application that used the aforementioned WRF infrastructure to configure storm-following nests at cloud-permitting or cloud-resolving scales (Davis et al. 2008, 2010; Dudhia et al. 2008; Fierro et al. 2009; Xiao et al. 2009).

Moving nests have also been successfully implemented in operational NWP models for TCs (Kurihara et al. 1998; Gopalakrishnan et al. 2006; Doyle et al. 2014; Tallapragada et al. 2014; Mehra et al. 2018). The first operational application of a storm-following nest at the National Oceanic and Atmospheric Administration (NOAA) was in the Geophysical Fluid Dynamics Laboratory (GFDL) hurricane model (Kurihara et al. 1998; Bender et al. 2007), which included two telescopic moving nests within a static, regional parent domain. The innermost nest achieved 1/6° resolution at a time when most global NWP models had resolutions on the order of ~1°. Although its resolution was later improved to 1/12° (~9 km), the GFDL hurricane model was too coarse to permit the simulation of clouds and convection, which inhibited its ability to produce reliable intensity and structure forecasts for TCs.

Gopalakrishnan et al. (2006) described the advancement of research-based moving nests in WRF for operational deployment at the NOAA/ National Weather Service (NWS)/ National Centers for Environmental Prediction (NCEP) using the Nonhydrostatic Mesoscale Model dynamical core (Janjić et al. 2001) within the WRF framework (called WRF-NMM). A key aspect of these moving nests is that they were configured on a rotated latitude–longitude grid,[1] allowing them to be positioned at higher latitudes without overstretching the grid or the need to adjust the time step to avoid numerical instability. Additionally, the nests resolve terrain at high resolution, including steeper slopes and higher peaks, for scenarios when TCs move near or over mountainous regions (e.g., Hispaniola, Taiwan, Hawaii).

[1] For more information about rotated grids in WRF, please see the documentation www2.mmm.ucar.edu/wrf/users/docs/user_guide_v4/v4.1/users_guide_chap3.html.

The moving nests described by Gopalakrishnan et al. (2006) became critical components of the Hurricane Weather Research and Forecasting (HWRF; Table 1) modeling system (Gopalakrishnan et al. 2011, 2012, 2013; Bao et al. 2012; Tallapragada et al. 2014; Atlas et al. 2015; X. Zhang et al. 2016; Mehra et al. 2018). The nests facilitated computationally efficient improvements to TC intensity and structure predictions in operations, and, consequently, HWRF is currently a premier operational NWP model for TC guidance at NOAA and around the world. For example, resolution refinements to moving nests in HWRF are computationally efficient even when configured at cloud-permitting resolutions (Tallapragada et al. 2014; X. Zhang et al. 2016; Gopalakrishnan et al. 2020). These resolution refinements have provided the capability for HWRF to improve intensity forecasts by accommodating additional upgrades to the model (e.g., physics parameterizations).

The goal of this study is to highlight the evolution and performance of high-resolution, storm-following nested grids in HWRF. This is timely because NOAA is currently developing moving nest technology to be implemented in the Hurricane Analysis and Forecast System

Table 1. Acronyms and definitions for models and experiments.

Acronym	Definition
HWRF	NOAA's Hurricane Weather Research and Forecasting modeling system
HWRFx	HWRF experimental modeling system
HWRF-B	Basin-scale HWRF modeling system
MS	Multistorm configuration of HWRF-B (default)
SS	Single-storm configuration of HWRF-B

(HAFS; Dong et al. 2020; Gopalakrishnan et al. 2020; Hazelton et al. 2021, 2022), the hurricane application of the Unified Forecast System[2] (UFS; National Weather Service 2017; Rood et al. 2018). UFS is a community-based, coupled, comprehensive NWP model for operational forecasts at NOAA and is based on the finite volume cubed-sphere (FV3) dynamical core (Lin and Rood 1996; Lin 2004; Harris and Lin 2013).

[2] For more details about UFS, please visit https://ufscommunity.org.

We will demonstrate forecast improvements that can be linked to the implementation of and upgrades to the moving nest technology in HWRF, and the results described herein will motivate similar developments in HAFS. First, moving nests in the operational HWRF are introduced, and the relationship between moving nest upgrades and HWRF forecast performance is evaluated. Next, the development of moving nests for multiple TCs is presented and the value added over a single-storm configuration is investigated. In particular, three different types of TC–TC interactions are explored, with an emphasis on TC communication through the synoptic-scale environment. Finally, the future of moving nest technology and recommendations for its implementation in HAFS is discussed.

Storm-following nests: Backbone of the operational HWRF model

With support from the multiagency Hurricane Forecast Improvement Project (HFIP; Gall et al. 2013; Gopalakrishnan et al. 2020), the TC community tested, evaluated, and, subsequently, improved moving nest technology in HWRF since it began running operationally at NOAA/NWS/NCEP in 2007. See the sidebar on "Hurricane Forecast Improvement Project" for more information about the establishment and priorities of the project. HWRF was initially configured with a static, regional parent domain at 27-km resolution that was two-way interactive with a single moving nest at 9-km resolution (Gopalakrishnan et al. 2011). At the Hurricane Research Division (HRD) in NOAA's Atlantic Oceanographic and Meteorological Laboratory (AOML), an experimental version of HWRF (HWRFx; Table 1; Zhang et al. 2011) was developed to target TC intensity forecast improvements. In HWRFx, a new nesting architecture was introduced that allowed for a telescopic (i.e., multilevel) nesting capability

Hurricane Forecast Improvement Project

The HFIP (Gall et al. 2013; Gopalakrishnan et al. 2020) is a national effort that coordinates U.S. federal agencies and academic institutions to collectively improve TC forecast guidance and our understanding of TC processes. The HFIP was established in 2008 to address the increasing vulnerability of the United States to devastating impacts from tropical cyclones. Congress set specific goals to achieve a 20% reduction in track and intensity forecast errors in 5 years and a 50% reduction in 10 years (see Fig. 1). HFIP has supported important collaborations across the tropical cyclone community, including NOAA entities, such as the Atlantic Oceanographic and Meteorological Laboratory, the Environmental Modeling Center and National Hurricane Center within NCEP, the Developmental Testbed Center, and academic institutions.

A priority of HFIP is to improve the HWRF modeling system, including the implementation of and further development of moving nest technology. In response to this goal, HWRFx was created to target TC intensity improvements through advancements to moving nest technology (Zhang et al. 2011), and HWRF-B was developed to feature the advanced moving nest technology for multiple TCs (X. Zhang et al. 2016; Alaka et al. 2020). HFIP facilitates the testing and evaluation of HWRF-B and other experimental models through the HFIP Real-Time Experiments (HREx). Through HREx, high-performance computing resources are secured annually during hurricane season on NOAA research and development supercomputers to test experimental models in an environment that mimics operations. HWRF-B has been a part of HREx every year since 2013, which has contributed to robust testing of the multistorm moving nest approach. The exposure that HFIP has brought to the moving nests is one of the reasons this technology is being transitioned to and developed further in HAFS. To support HAFS and future TC forecast efforts, HFIP was re-established as the Hurricane Forecast Improvement Program under the Weather Research and Forecasting Innovation Act of 2017 (U.S. Public Law 115-25). More details about HFIP can be found in Gall et al. (2013) and Gopalakrishnan et al. (2020), as well as at https://hfip.org.

and an efficient centroid-based nest movement algorithm. As a result, a second moving nest with a resolution of 3 km was implemented into HWRF in 2012, marking the first time that an operational NWP model was configured with cloud-permitting resolutions for TC forecasting (Tallapragada et al. 2014; Goldenberg et al. 2015). The inner moving nest is positioned within the outer moving nest, and both nests remain centered on the TC position throughout the model integration (online supplemental Fig. 1; https://doi.org/10.1175/BAMS-D-20-0134.2). The triple domain configuration is still used in the operational HWRF to this day, and the longevity of this configuration is evidence of its ability to produce increasingly useful TC forecast guidance as the model is upgraded every year.

Verification of operational HWRF forecasts for all North Atlantic TCs indicated that intensity improvements were linked to the implementation of the inner moving nest and the progressive refinement of model resolution (Fig. 1), consistent with the findings of Tallapragada et al. (2014). Specifically, Fig. 1 includes intensity forecast errors and skill for four different versions of the operational HWRF: 1) the 2011 version (two domains; one moving nest at 9 km), 2) the 2012 version (three domains; two moving nests at 9 and 3 km), 3) the 2015 version (three domains; two moving nests at 6 and 2 km), and 4) the 2018 version (three domains; two moving nests at 4.5 and 1.5 km). The corresponding resolution of the HWRF parent domain was always adjusted to maintain a 3:1 ratio with the outer moving nest. Each version of HWRF was verified independently to account for year-to-year variability, leading to a heterogenous sample (Table 2).

The 2018 version of HWRF had the lowest absolute intensity forecast errors at every forecast lead time except for 96 h (Fig. 1a). It is evident that absolute intensity forecast errors did not decrease at every lead time with every model upgrade. Intensity forecast errors are difficult to compare for different years because the number of verifiable forecasts vary by year and TC intensity could be easier to predict in some years and harder to predict in others. For this reason, intensity forecast skill scores were computed using climatology and persistence (OCD5) as a baseline to account for the degree of difficulty each hurricane season presented for TC intensity predictions. The 2018 version of HWRF had the highest intensity forecast skill at 24 h and longer forecast lead times (Fig. 1b). Remarkably, intensity forecast skill scores improved for each successive version of HWRF at 48 h and longer forecast lead times, providing evidence that each moving nest upgrade was associated with intensity forecast improvements (Fig. 1b). It is important to note that the HWRF versions evaluated in this study featured other changes in addition to moving nest upgrades, including upgrades to model dynamics and physics (e.g., Gopalakrishnan et al. 2020). Therefore, the percentage of intensity forecast improvement that was attributed to moving nest upgrades alone could not be determined. This gap motivated controlled experiments in the following section to target the isolated impact of moving nests on TC forecasts.
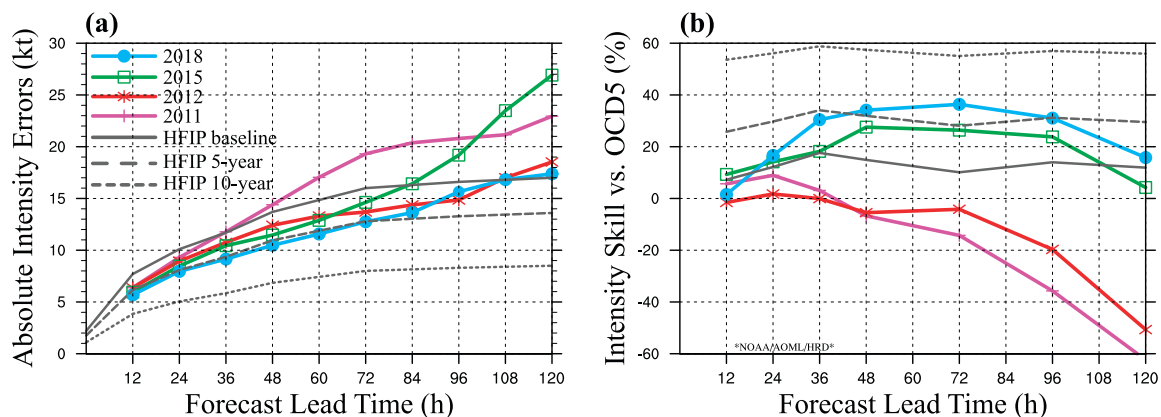

Fig. 1. (a) Intensity forecast errors (kt) and (b) intensity forecast skill (%) relative to climatology and persistence (OCD5). In both panels, the 2018 operational HWRF (blue, circle), the 2015 operational HWRF (green, square), the 2012 operational HWRF (red, asterisk), and the 2011 operational HWRF (pink, cross) are shown alongside the HFIP baseline (solid gray), 5-yr goal (long dashed gray), and 10-yr goal (short-dashed gray).

Table 2. The sample size is shown for different versions of the operational HWRF (2011, 2012, 2015, 2018) at 12–120-h forecast lead times.

HWRF version	Forecast lead time (h)									
	12	24	36	48	60	72	84	96	108	120
2011	378	360	335	307	280	254	229	206	188	167
2012	424	397	365	338	307	278	252	228	206	187
2015	217	210	197	179	163	145	129	114	99	82
2018	382	363	339	310	283	257	232	212	192	174

The HFIP baseline, 5-yr goals, and 10-yr goals are also shown in Fig. 1, as described by Gall et al. (2013) and Gopalakrishnan et al. (2020). The HFIP baseline was established by NOAA's National Hurricane Center (NHC) to represent average errors from operational models over a 3-yr period (2006–08), including HWRF (Gall et al. 2013). The 5-yr goal represents a 20% error reduction from the baseline errors, and the 10-yr goal represents a 50% error reduction (see the sidebar on "Hurricane Forecast Improvement Project"). The 2011 and 2012 versions of HWRF had intensity forecast skill scores that were well below the HFIP baseline and were negative at 48 h and longer lead times. The 2015 version of HWRF beat the HFIP baseline at most lead times, and the 2018 version of HWRF beat the 5-yr HFIP goal at 48 and 72 h. Readers are reminded that the HFIP baseline is not an HWRF baseline, and intensity forecasts from the 2011 version of HWRF were far inferior to the HFIP baseline that was established three years prior to 2011. The HFIP baseline and goals serve as a reminder that HWRF intensity forecasts have much room for improvement to meet TC community expectations.

High-resolution nests for multiple storms

The basin-scale HWRF modeling system and experimental design. Although upgrades to the moving nest configuration in the operational HWRF was associated with notable intensity forecast improvements, HWRF is still limited in its ability to realistically capture the interaction between multiple TCs (Alaka et al. 2017). The operational HWRF is a TC-centric modeling system, i.e., it only simulates one TC at high resolution per forecast integration. Previous studies investigated TC–TC interactions and the importance of these interactions to TC forecasts (Fujiwhara 1921; Brand 1970; Dong and Neumann 1983; Lander and Holland 1993; Aberson and DeMaria 1994;
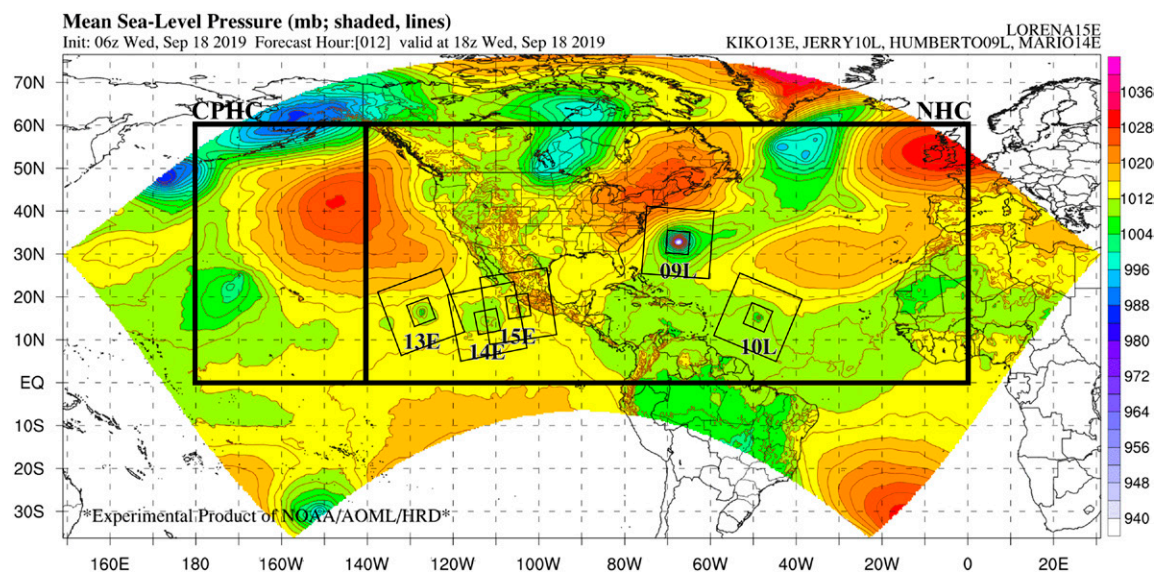

Fig. 2. Mean sea level pressure (hPa) is shown for 12 h into an HWRF-B forecast initialized at 0600 UTC 18 Sep 2019. The extent of the HWRF-B parent (i.e., outermost) domain is also shown. Five TCs were configured with high-resolution moving nests (shown as boxes with thin black lines centered on each TC): Humberto (09L), Jerry (10L), Kiko (13E), Mario (14E), and Lorena (15E). Boxes with thick black outlines mark the areas of responsibility for NOAA's National Hurricane Center (NHC; eastern box) and Central Pacific Hurricane Center (CPHC; western box).

Carr et al. 1999; Aberson 2011; Archambault et al. 2013, 2015; Susca-Lopata et al. 2015; X. Zhang et al. 2016; Alaka et al. 2017, 2020). Three different types of TC–TC interactions were identified in Alaka et al. (2017) and were investigated in high-definition model forecasts in the present study: direct (e.g., the Fujiwhara effect or binary interactions), indirect (e.g., environmental outflow interactions), and remote (e.g., modulation of global-scale flow).

To address the TC-centric limitation of the operational HWRF, an experimental version of HWRF, known as the Basin-scale HWRF (HWRF-B; Table 1; X. Zhang et al. 2016; Alaka et al. 2017, 2019, 2020), was developed at AOML/HRD in collaboration with the Environmental Modeling Center (EMC) in NOAA's NCEP and the Developmental Testbed Center (DTC). HWRF-B was created, in part, to showcase HWRF's moving nest technology for multiple TCs in the same forecast. It is the first NWP model to be configured with high-resolution moving nests for multiple TCs in the same model integration. The 2020 version of HWRF-B includes all configuration options present in the corresponding version of the operational HWRF (Biswas et al. 2018). HWRF-B differs from HWRF in that it is configured with up to five TC-following nests within a large, static parent domain that includes most of the areas of responsibility of NHC and NOAA's Central Pacific Hurricane Center (CPHC) (Fig. 2). For that reason, the HWRF-B configuration is also known as the "multistorm" configuration (MS; Table 1). Details of the MS configuration were discussed in Alaka et al. (2020). For each TC, associated moving nests are two-way interactive with each other and with the parent domain, and this configuration choice is paramount to the simulation of TC–TC and multiscale interactions necessary for accurate intensity forecasts.

To evaluate the impact of moving nests on TC forecasts, HWRF-B was modified to only allow moving nests for one TC per model integration, similar to the operational HWRF. For simplicity, this modified HWRF-B configuration will also be referred to as the "single-storm" configuration (SS; Table 1). The only difference between the MS and SS configurations was the number of moving nests per model integration. Therefore, more model integrations were required for SS to produce the same number of TC forecasts as MS. This is the first time that a systematic experiment has been conducted to evaluate the impact of the number of moving nests on TC track, intensity, and size. In total, 451 verifiable forecasts were compared for MS and SS for the 2018 and 2019 hurricane seasons in the North Atlantic and eastern North Pacific Oceans. Because each hurricane season contains several TCs of varying importance, NHC identified priority
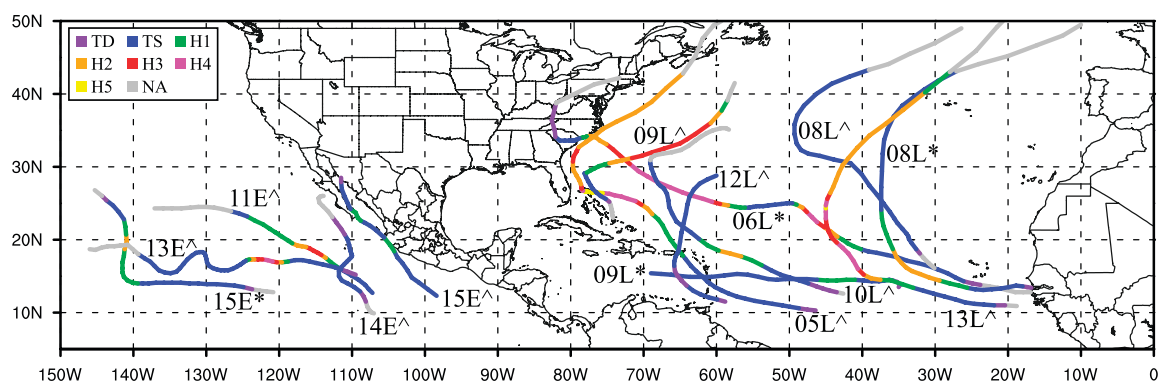

Fig. 3. Best track positions and maximum intensities are shown for all fourteen TCs included in the multistorm and single-storm HWRF-B experiments. Best track intensities are color-coded based on the following classifications: tropical depression (TD; purple), tropical storm (TS; blue), category 1 hurricane (H1; green), category 2 hurricane (H2; orange), category 3 hurricane (H3; red), category 4 hurricane (H4; magenta), and category 5 hurricane (H5; yellow). Non-TC classifications are shown in gray (NA). TCs from 2018 are marked with an asterisk and those from 2019 are marked with a caret. The TCs, in order of when they were first classified as such, include Miriam (15E*), Florence (06L*), Helene (08L*), Isaac (09L*), Dorian (05L^), Juliette (11E^), Gabrielle (08L^), Kiko (13E^), Humberto (09L^), Mario (14E^), Lorena (15E^), Jerry (10L^), Karen (12L^), and Lorenzo (13L^). See Table 3 for information about each TC.

Table 3. Tropical cyclones (TCs) simulated in both HWRF-B experiments in chronological order of when they were first classified by the National Hurricane Center. TCs in the same group had overlapping life cycles.

Name	Year	Basin	Storm ID	Group
Miriam	2018	Eastern North Pacific	15E	1
Florence	2018	North Atlantic	06L	1
Helene	2018	North Atlantic	08L	1
Isaac	2018	North Atlantic	09L	1
Dorian	2019	North Atlantic	05L	2
Juliette	2019	Eastern North Pacific	11E	2
Gabrielle	2019	North Atlantic	08L	2
Kiko	2019	Eastern North Pacific	13E	3
Humberto	2019	North Atlantic	09L	3
Mario	2019	Eastern North Pacific	14E	3
Lorena	2019	Eastern North Pacific	15E	3
Jerry	2019	North Atlantic	10L	3
Karen	2019	North Atlantic	12L	3
Lorenzo	2019	North Atlantic	13L	3

TCs (A. Penny 2020, personal communication), and at least two priority TCs had to be active at the same time to be included in this study. Fourteen TCs were included in this study, with nine in the North Atlantic basin and five in the eastern North Pacific basin (Table 3). Positions and maximum intensities from the NHC postprocessed best track (Rappaport et al. 2009) represented the ground truth for the TCs evaluated in this study (Fig. 3). These TCs represented three groups with overlapping life cycles (Table 3): 1) Miriam, Florence, Helene, and Isaac; 2) Dorian, Juliette, and Gabrielle; and 3) Kiko, Humberto, Mario, Lorena, Jerry, Karen, and Lorenzo. These three groups included several different types of TC–TC interactions, including direct, indirect, and remote interactions. The analysis later in this section will focus on the third group of TCs to illustrate the different types of interactions. It is noted that the MS configuration produced forecasts for additional, nonpriority TCs. However, SS did not produce forecasts for these nonpriority TCs, and, therefore, they did not factor into the results of this study.

Comparing the performance of multistorm and single-storm configurations. TC intensity forecasts produced by MS and SS in the North Atlantic and eastern North Pacific were verified to determine the sensitivity to the number of TCs configured with moving nests (i.e., one TC versus multiple TCs). A forecast was verified if the system was classified as a TC at the initial time and at the verification time.[3] In addition, the verification performed in this study excluded model forecast or NHC best track positions over land because intensity errors can be drastically different for a TC that is just onshore versus just offshore and the focus of this work was on TC–TC interactions rather than TC-land interactions. These rules were applied to all verification statistics in this study.

[3] For more details, please visit www.nhc.noaa. gov/verification/verify2.shtml.

Verification statistics revealed notable improvement of intensity forecasts in MS compared with SS, especially at longer lead times (Figs. 4a,c). In fact, MS average absolute intensity errors were significantly lower than those from SS at the 95% confidence level at a lead time of 84 h, reflected by MS forecast skill near 10%. Overall, MS intensity forecast skill scores were 5%–10% at lead times of 60 h and greater, indicating that benefits from moving nests for multiple TCs do not occur instantaneously. Intensity forecast errors were quite similar at lead times of 48 h and shorter, with a slight downward trend in MS forecast skill in the first 36 h. Many operational TC model upgrade decisions, including for HWRF, are based on statistically insignificant results, even when the sample size exceeds 500 cases. Therefore, we encourage readers to focus on discernable differences in verification statistics between MS and SS.

Intensity forecasts were then stratified by the number of TCs at the model initialization time because moving nests were only configured for TCs that were active at the start of a forecast
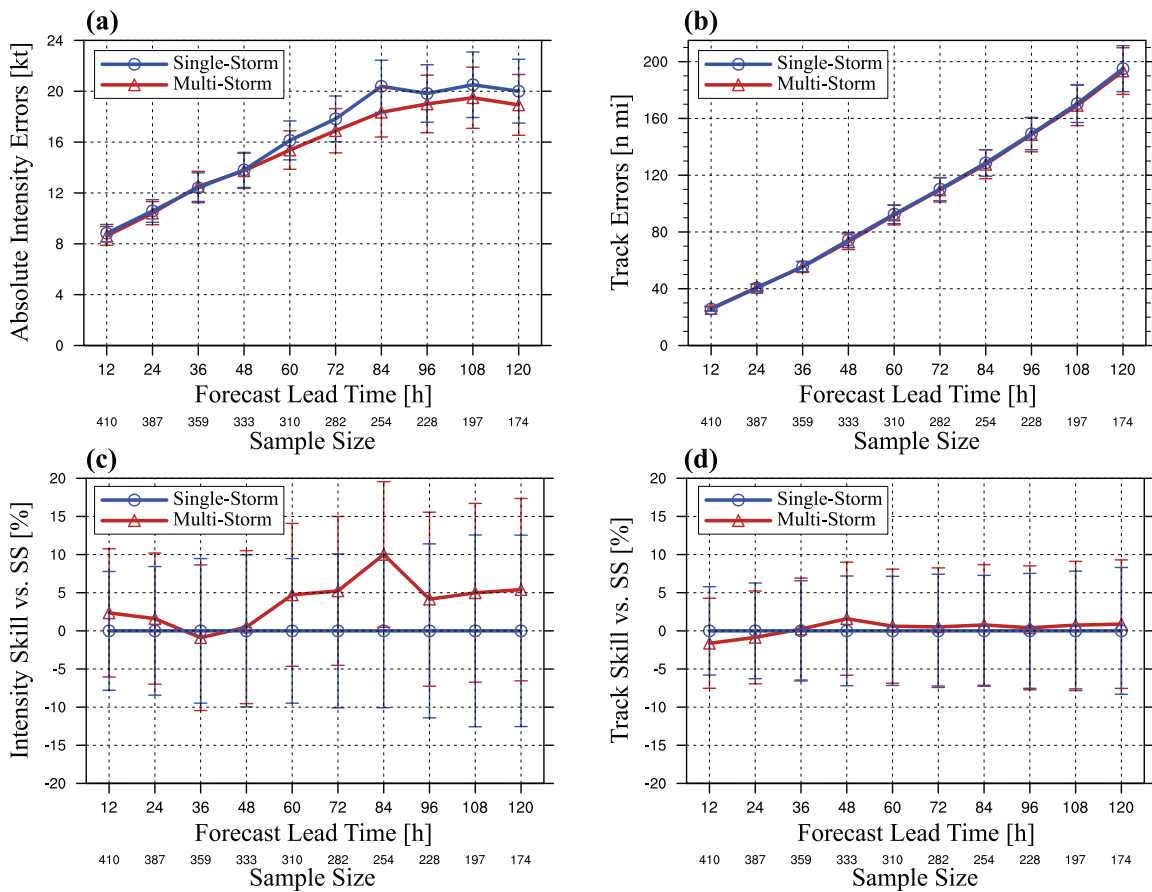
Fig. 4. The HWRF-B multistorm configuration (MS; brown triangle) and the HWRF-B single-storm configuration (SS; blue circle) are compared for (a) absolute intensity forecast errors (kt), (b) track forecast errors (n mi; 1 n mi = 1.852 km), (c) intensity forecast skill scores vs SS (%), and (d) track forecast skill scores vs SS (%). Verification statistics are shown for 12–120-h lead times with an interval of 12 h. Skill scores are computed using SS as the reference model and represents percent improvement/degradation of MS relative to SS. The sample size at each forecast lead time is available below each panel. The 95% confidence interval is represented by whiskers.

(i.e., nests were not spawned during the model integration). Intensity forecasts were notably improved when moving nests were configured for five TCs compared to forecasts with moving nests for fewer TCs (Fig. 5). With five sets of moving nests, MS intensity forecast skill was significant at lead times of 60−84 h and showed 7%−14% improvement over SS at all lead times
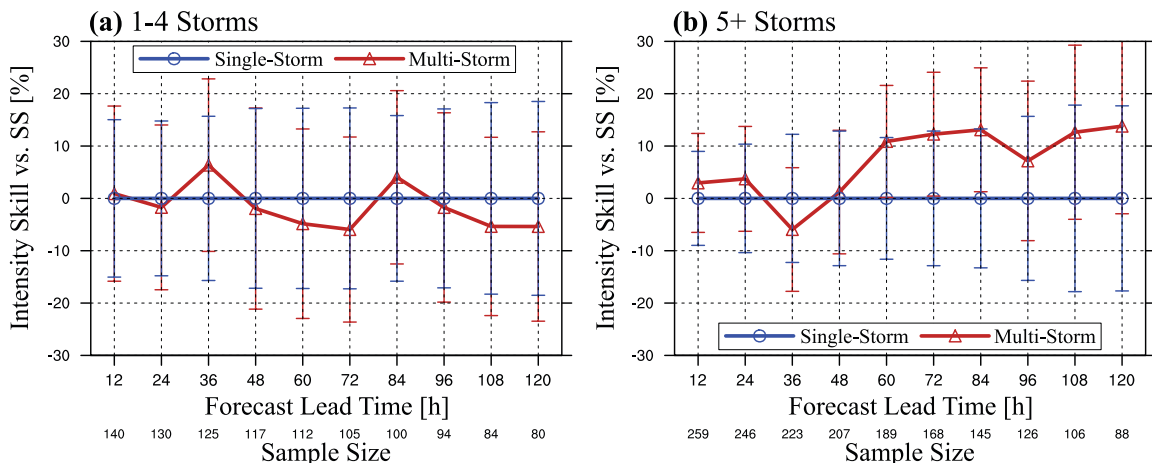
Fig. 5. As in Fig. 4c, but stratified for (a) 1–4 TCs at the initial forecast time and (b) 5 or more TCs at the initial forecast time.
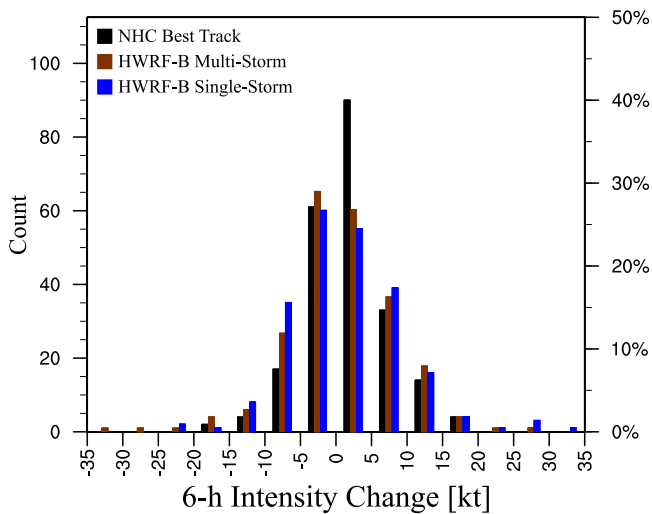
Fig. 6. Six-hour intensity changes (kt) are shown for the NHC best track (black; left bar), HWRF-B MS (brown; middle bar), and HWRF-B SS (blue; right bar) for 5-kt bins. MS and SS are shown for 96-h forecasts and the NHC best track is shown for corresponding valid times. The left _y_ axis represents the total count in each bin, and the right _y_ axis represents the percentage of the total sample.

greater than or equal to 60 h (Fig. 5b). When MS was configured with moving nests for fewer than five TCs, MS intensity forecast skill was between −5% and 5% with no statistically significant lead times. It is noted that the sample was dominated by forecasts with at least five TCs, which accounted for 65% of verifiable forecasts at a lead time of 12 h. Intensity forecasts showed some improvement when the number of TCs with nests was increased from one to four, although the number of cases was relatively small (not shown). TC size, measured by 10-m wind radii [maximum, 34 kt, 50 kt, and 64 kt (1 kt ≈ 0.51 m s⁻¹)], was modestly improved in MS forecasts compared with SS forecasts at most lead times, as well (not shown).

Track forecasts were very similar between the two configurations, with a slight, insignificant edge (1%–2% improvements) for MS at lead times greater than or equal to 48 h (Figs. 4b,d). Recent studies have shown that previous versions of HWRF-B improved track forecasts relative to the operational HWRF (Alaka et al. 2017, 2020). In particular, Alaka et al. (2017) found that HWRF-B track forecast skill improved the most for remote TC–TC interactions, and Alaka et al. (2020) showed that HWRF-B track forecast skill improved at longer lead times when the number of storms increased. B. Zhang et al. (2016) added that only increasing the size of the outermost domain in HWRF improved track forecasts. In support of this previous work, the track forecast statistics shown in Fig. 4 indicate that track forecasts are similar when the outermost domain size is identical, i.e., as in MS and SS. Average TC track performance from MS and SS was also similar for each type of TC–TC interaction, and, for this reason, the evaluation focused on intensity forecast performance.

The 6-h intensity change is compared for the NHC best track, MS, and SS (Fig. 6). The intensity change is shown for a lead time of 96 h for the models and corresponding valid times from the NHC best track, although the results are similar at other lead times. Note that 5-kt bins for intensity change were used to reflect that intensity from the NHC best track is reported in 5-kt increments. The distribution of intensity change in MS forecasts was more similar to the NHC best track than in SS forecasts. In particular, the percentage of MS intensity change forecasts from −5 to 5 kt (56%) was closer to the NHC best track (67%) than in SS (50%), although both HWRF-B configurations underestimated the total number shown by the NHC best track in these bins. The distribution of intensity change forecasts in SS was generally broader than in MS, with 47% in the bins from −5 to −15 kt and 5–15 kt for SS and 41% for MS. MS was in better agreement with the NHC best track (31%).

Exploration of TC–TC interactions. HWRF-B was used to investigate differences in TC–TC interactions based on the number of TCs configured with moving nests (i.e., one versus many). As noted earlier, Alaka et al. (2017) and others identified three types of TC–TC interactions: direct, indirect, and remote. Case studies of TC–TC interactions were explored for the third group of TCs (Table 3) because it represented a data-rich period that included all types of interactions.
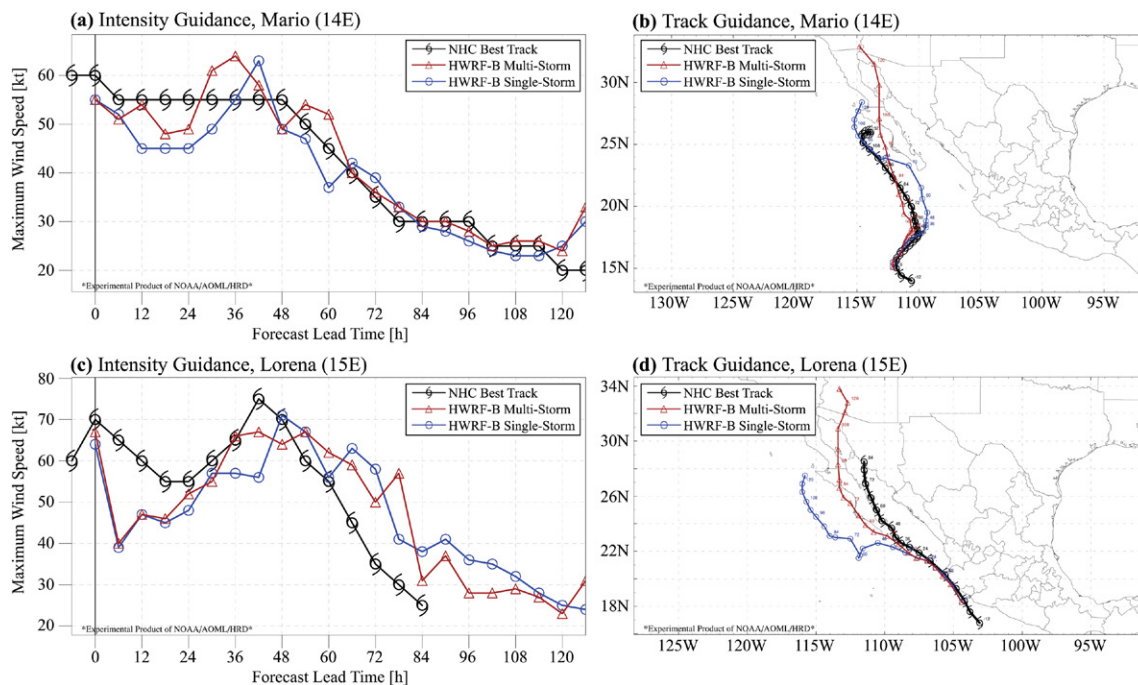
Fig. 7. (a) Maximum wind speed (kt), i.e., intensity forecasts and (b) track forecasts of Tropical Storm Mario (14E) initialized at 0000 UTC 19 Sep 2019 for HWRF-B MS (brown triangle), HWRF-B SS (blue circle), and the NHC best track (black TC symbol). (c),(d) As in (a) and (b), but for Hurricane Lorena (15E).

DIRECT TC–TC INTERACTIONS. Direct TC–TC interactions are also known as binary interactions or the "Fujiwhara effect," named for the pioneering laboratory experiments conducted by Sakuhei Fujiwhara (Fujiwhara 1921). Direct interactions typically occur when two TCs are within 1,500 km of one another and begin to rotate around each other (Brand 1970). In the classic Fujiwhara model, the two TCs engaged in a direct interaction will eventually merge into a single vortex. Although direct interactions are typically thought of as the leading example of TC–TC interaction, they are relatively uncommon. Dong and Neumann (1983) documented an average of only 0.33 yr^{-1} in the North Atlantic basin. Furthermore, TCs in the real atmosphere do not necessarily behave as they do in idealized simulations, meaning TCs are more likely to rotate around one another without merging, and the TC–TC interactions that actually qualify as direct are not always obvious (Lander and Holland 1993).

Verification statistics were stratified for forecasts with direct TC–TC interactions (i.e., two TCs less than 1,500 km apart) at the model initialization time (not shown). MS intensity forecasts improved by 5%–30% at forecast lead times greater than or equal to 60 h compared with SS. Some intensity forecast degradation was observed at forecast lead times shorter than 60 h, suggesting potential issues related to the initialization of nests that is discussed later. On average, MS track forecasts generally did not improve compared with SS for TC–TC interactions. It is noted that ~16% of verifiable 12-h forecasts featured direct TC–TC interactions, and, consequently, MS forecast skill was insignificant at every analyzed forecast lead time.

The two HWRF-B configurations (MS and SS) included forecasts of a direct TC–TC interaction between Tropical Storm Mario (14E) and Hurricane Lorena (15E) (e.g., Avila 2019; Berg 2019). This interaction did not result in a merger of the two TCs, and, thus, it did not follow the classic Fujiwhara model. Both TCs were located near the western Mexico coast in the eastern North Pacific Ocean, with Lorena right along the coastline and Mario generally to the southwest of Lorena. The weaker Mario rotated clockwise to the northeast toward Lorena
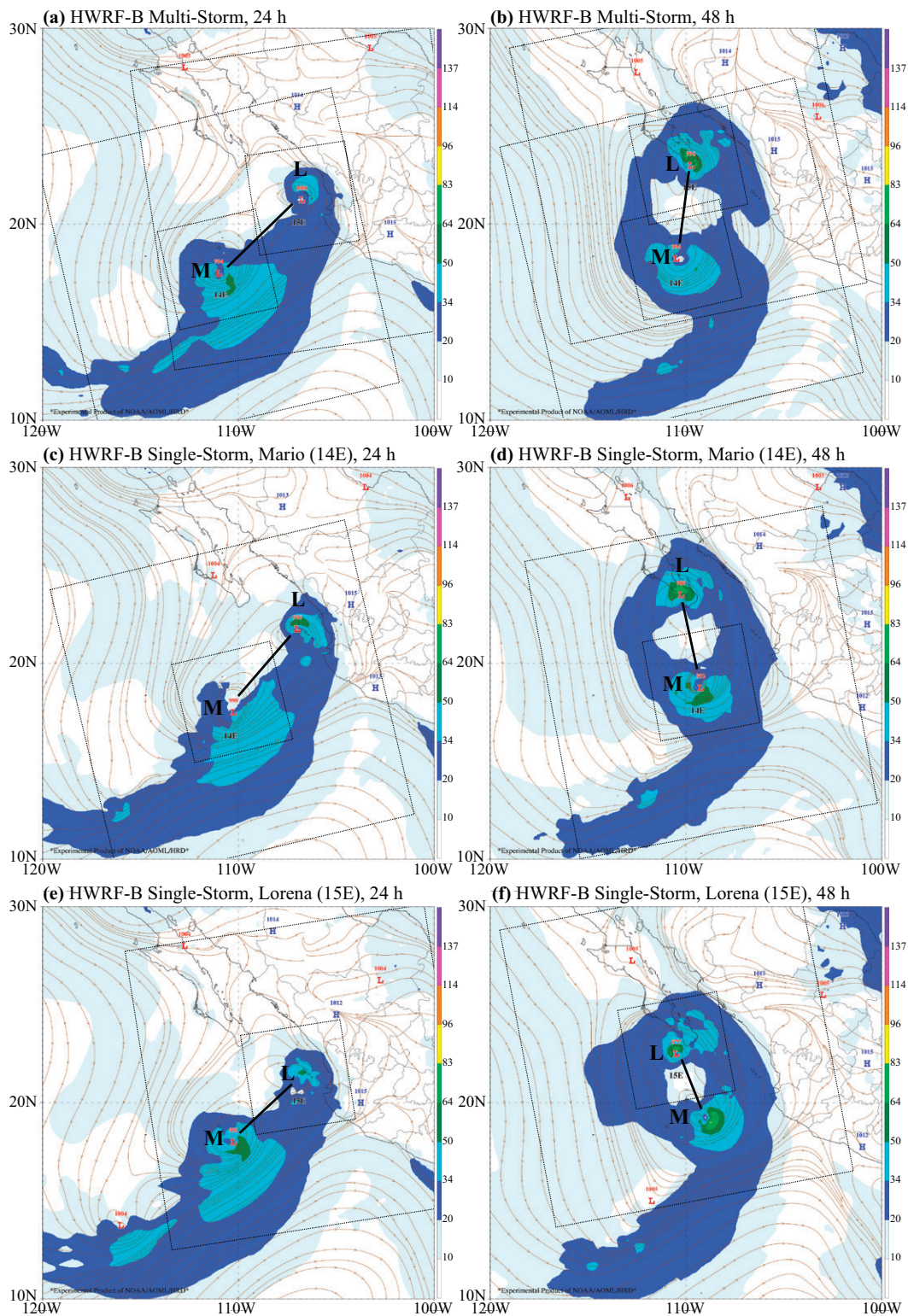
Fig. 8. For forecasts initialized at 0000 UTC 19 Sep 2019, 850-hPa wind magnitude (shading; kt) and streamlines are shown from (a),(b) HWRF-B multistorm, (c),(d) HWRF-B single storm with high-resolution nests for Mario only, and (e),(f) HWRF-B single storm with high-resolution nests for Lorena only. (left) The 24-h forecast lead times and (right) 48-h forecast lead times. The position of Mario is labeled by "M," and the position of Lorena is labeled by "L." Moving nests are shown in thin, dotted black lines. A thick black line shows the axis between Mario and Lorena.

and the stronger Lorena turned slightly counterclockwise to the west-northwest toward Mario (see 14E^ and 15E^ in Fig. 3). Maximum intensity forecasts from MS and SS were remarkably similar throughout the forecast period (Figs. 7a,c), although accumulated errors from MS were

slightly lower in both cases. However, the track forecasts revealed notable differences, with lower errors in MS than in SS for both TCs (Figs. 7b,d).

The 850-hPa wind fields for Mario and Lorena were intertwined, with no discernible gap in the 20–34-kt winds between the two TCs (dark blue in Fig. 8). In fact, 850-hPa streamlines were observed to encompass both TCs as they rotated around one another. Upon closer inspection, the 850-hPa wind field for these two TCs showed subtle, but important, differences between the two experiments. In MS, Mario had a broad area of 34-kt winds at a lead time of 48 h and Lorena was very small with hurricane-force winds at the same time (Fig. 8b). In the SS forecasts (Figs. 8c–f), both Mario and Lorena had wind fields that were broader at 48 h (e.g., 50-kt winds shown in dark green in Fig. 8), leading the two TCs to rotate farther around one another than what was observed in reality (see NHC best track in Figs. 2, 7). In MS, the centers of Mario and Lorena rotated by 36.2° in the counterclockwise direction from 24 to 48 h. In the SS simulation for Mario, the TC centers rotated by 55.2°, and, in the SS simulation for Lorena, the TC centers rotated by 70.3°. In the NHC best track, Mario and Lorena rotated by 27.0° in the same 24-h period. The smaller degree of rotation in MS was more consistent with the NHC best track.

These forecasts highlight the importance of moving nests for multiple TCs not only to improve intensity forecasts, but also track and structure forecasts for TCs in close proximity. Two-way interactions between the moving nests and the parent domain allowed for the communication of high-resolution wind fields associated with each TC. If one of the TCs was not simulated at cloud-permitting scales with high-resolution moving nests, its wind field could be too broad and the binary interaction with the high-resolution TC was unrealistically strong. It should be noted both TCs were simulated with at least 4.5-km resolution in the SS forecasts because their close proximity allowed both to reside within the outer moving nest of the other TC (Figs. 8c–f). However, the lack of an inner moving nest at 1.5-km resolution for both TCs inhibited the accurate prediction of wind structure and, consequently, the ensuing direct interaction.

INDIRECT TC–TC INTERACTIONS THROUGH UPPER-TROPOSPHERIC OUTFLOW. HWRF-B is well equipped to study indirect TC–TC interactions. The way in which moving nests communicate with one another through the parent domain is an analog to how the outflow of one TC modulates the synoptic-scale environment that can then influence another TC. In other words, indirect TC–TC interactions are a multiscale problem, with the vortex scale modulating the synoptic scale and vice versa. This is especially true for interactions between TCs that are 1,500–3,000 km apart from one another because they are too far apart to engage in direct interactions and are close enough to interact with the same synoptic-scale features.

Verification statistics were stratified for forecasts that included indirect TC–TC interactions at the model initialization time (not shown). Approximately 71% of verifiable forecasts had at least one instance of TCs that were 1,500–3,000 km apart that were capable of engaging in indirect interactions. MS forecasts improved relative to SS forecasts with at least one instance of indirect TC–TC interaction, with insignificant improvements of 2%–10% at most lead times. When there were at least two instances of indirect TC–TC interactions, MS intensity forecasts improved by 8%–18% at forecast lead times greater than or equal to 60 h compared with SS, with significant (95%) skill at 60 h. MS and SS track forecast errors were generally comparable, with insignificant MS track forecast skill at every analyzed lead time.

A case study was performed on MS and SS forecasts initialized at 0000 UTC 19 September 2019, in which Hurricane Humberto and Tropical Storm Jerry indirectly interacted with one another. Humberto was a large, powerful hurricane that was beginning its extratropical transition in the northern North Atlantic (Stewart 2020) and Jerry was a smaller tropical storm that was predicted to intensify as it moved west-northwest toward the northern Lesser

Antilles (Brown 2019). MS included high-resolution moving nests for both TCs, whereas this particular forecast from SS included moving nests for Jerry and represented Humberto at relatively coarse resolution in the parent domain.

MS and SS track and intensity forecasts for Jerry were notably different, with MS producing a more accurate intensity and track forecast than SS (Fig. 9). In MS, Jerry achieved a maximum intensity of 85 kt at a lead time of 24 h, which was quite close to the NHC best track maximum intensity of 90 kt at the same time (Fig. 9a). Conversely, SS incorrectly intensified Jerry into a major hurricane, reaching a maximum intensity of 113 kt (i.e., nearly a category 4 hurricane) before weakening later on. Although track forecasts from both experiments had Jerry too far west, MS was closer to the NHC best track (Fig. 9b).

Upper-tropospheric potential vorticity[4] (PV) from the GFS analysis valid at 0000 UTC 20 September 2019 showed four features of interest (Fig. 10a): 1) Humberto in the northern North Atlantic (39°N, 59°W), 2) Jerry to the east of the Lesser Antilles (18°N, 57°W), 3) a large extratropical trough located just east of the U.S. mid-Atlantic coastline (36°N, 70°W), and 4) a tropical upper-tropospheric trough situated between Humberto and Jerry (25°N, 56°W). Over time, the tropical upper-tropospheric trough (feature 4) moved eastward and was absorbed into a larger trough (centered near 20°N and 40°W in Fig. 10a) as an anticyclonic wave breaking event occurred (not shown). Previous studies have highlighted the common occurrence of anticyclonic wave breaking events equatorward of the subtropical jet during the hurricane season (Homeyer and Bowman 2013; Papin et al. 2020). The wave breaking event is not discussed further because it occurred after Humberto has dissipated. However, the southwesterly flow associated with Hurricane Humberto and the large extratropical trough facilitated the indirect TC–TC interaction with Jerry enroute to initiating the aforementioned wave breaking event.

---

[4] PV is the product of absolute vorticity and static stability divided by density (https://glossary.ametsoc.org/wiki/Potential_vorticity).

At a lead time of 24 h, the synoptic-scale environment near Humberto and Jerry revealed two key differences between MS and SS that had implications for Jerry's forecast (Fig. 10b): 1) Humberto was more intense in the MS simulation due to high-resolution moving nests, leading to higher PV on the eastern edge of a large extratropical trough at the top of Fig. 10b and 2) the tropical upper-tropospheric trough north of Jerry was shifted south and east in MS, bringing higher PV closer to Jerry's circulation and halting intensification at an earlier time (Fig. 9a). These differences exceeded 1 PV unit (PVU; 1 PVU = 1×10^{-6} m^2 s^{-1} K kg^{-1}). Humberto had a maximum wind speed of 66 kt and a minimum central pressure of 968 hPa in MS compared to 55 kt and 983 hPa in SS. Overall, the presence of a more intense Humberto in MS strengthened southwesterly flow to
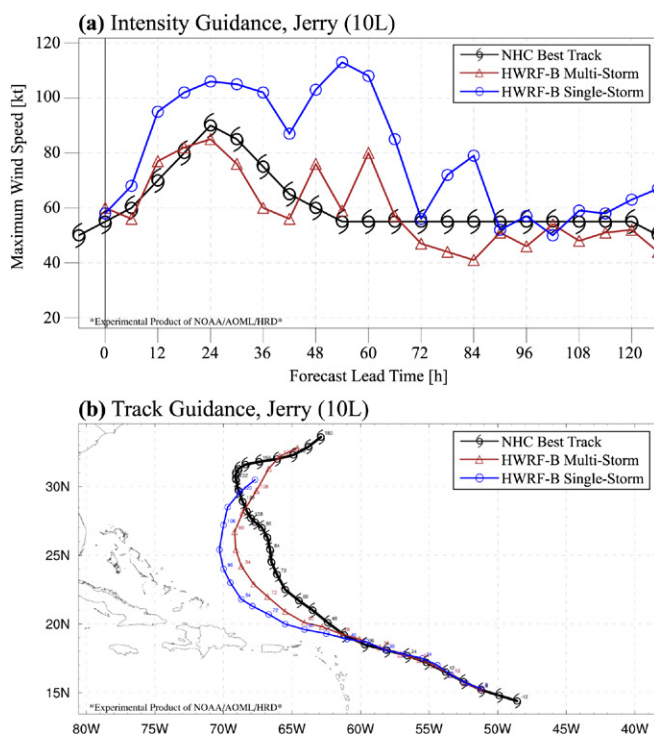

Fig. 9. (a) Maximum wind speed (kt), i.e., intensity forecasts and (b) track forecasts of Tropical Storm Jerry (10L) initialized at 0000 UTC 19 Sep 2019 for HWRF-B MS (brown triangle), HWRF-B SS (blue circle), and the NHC best track (black TC symbol).

its south, with zonal wind differences of up to 10 kt (Fig. 10c). This enhanced flow forced the tropical upper-tropospheric trough to interact with Jerry at an earlier time. On the other hand, a weaker Humberto in SS was associated with weaker southwesterly flow, and the tropical upper-tropospheric trough was consequently positioned farther north and west, as supported by PV and zonal wind differences (Figs. 10b,c). Therefore, the upper-tropospheric trough interacted with Jerry at a later time in SS, allotting additional time for Jerry to intensify to major hurricane status.

A TC can indirectly interact with another TC through dynamic or thermodynamic pathways. These two pathways were illustrated for the impact of Humberto on Jerry by deep-layer vertical wind shear (Figs. 11a,b) and midtropospheric relative humidity (Figs. 11c,d). Vertical
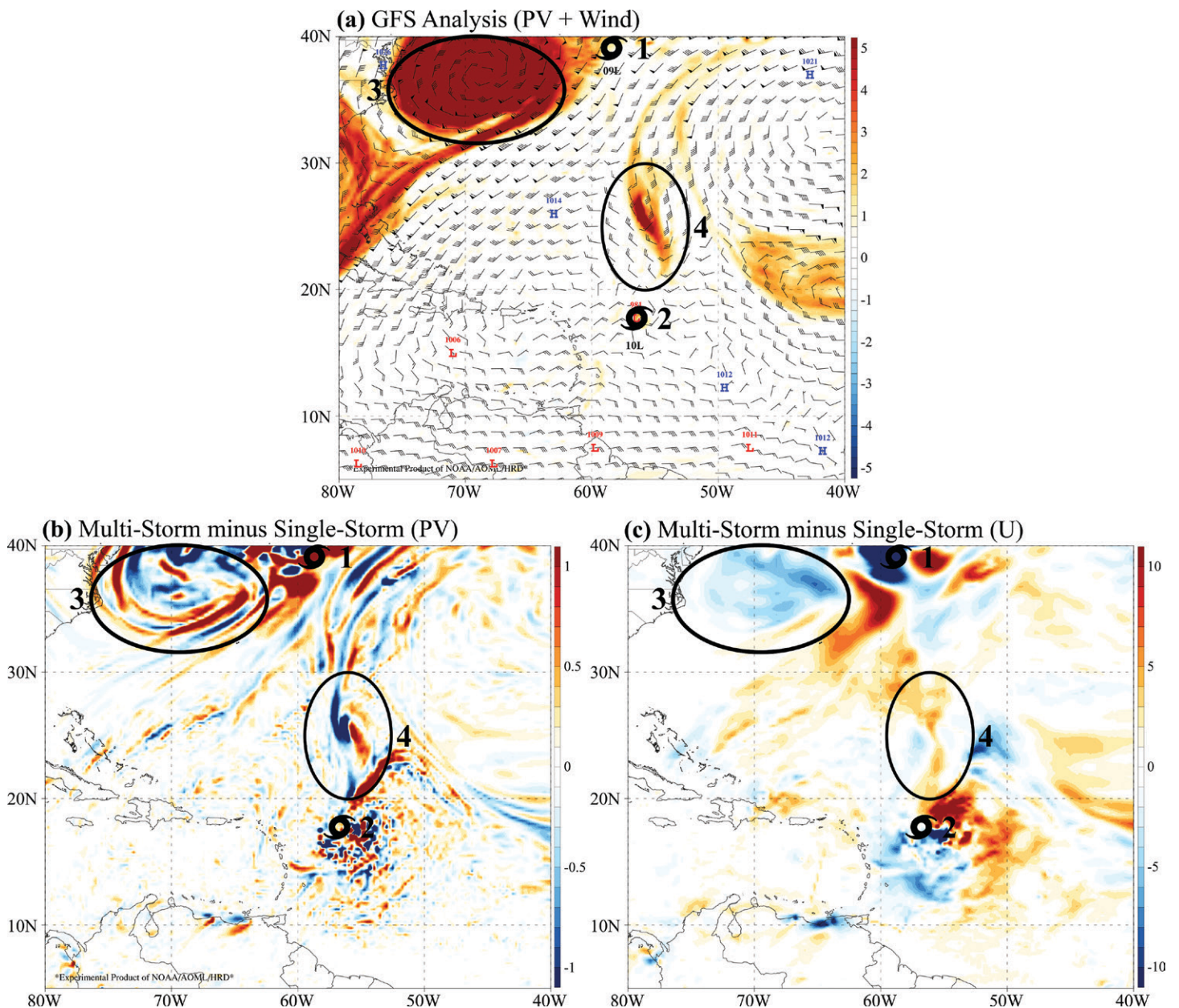
Fig. 10. (a) Large-scale 200-hPa potential vorticity (PV; 10^{-6} m^2 s^{-1} K kg^{-1}; shading), 200-hPa wind barbs (kt), and mean sea level pressure (MSLP; hPa) extrema from the GFS analysis at a valid time of 0000 UTC 20 Sep 2019. (b) Differences in 200-hPa PV are shown for HWRF-B MS minus HWRF-B SS at a lead time of 24 h from forecasts initialized at 0000 UTC 19 Sep 2019. (c) As in (b), but for the zonal component of the 200-hPa wind (U; kt). Four features of interest are labeled/circled in each panel: 1) Hurricane Humberto (39°N, 59°W), 2) Hurricane Jerry (18°N, 57°W), 3) a large extratropical trough (36°N, 70°W), and 4) a tropical upper-tropospheric trough (25°N, 56°W). SS has moving nests for Jerry only, while MS has high-resolution moving nests for multiple TCs, including Humberto and Jerry.
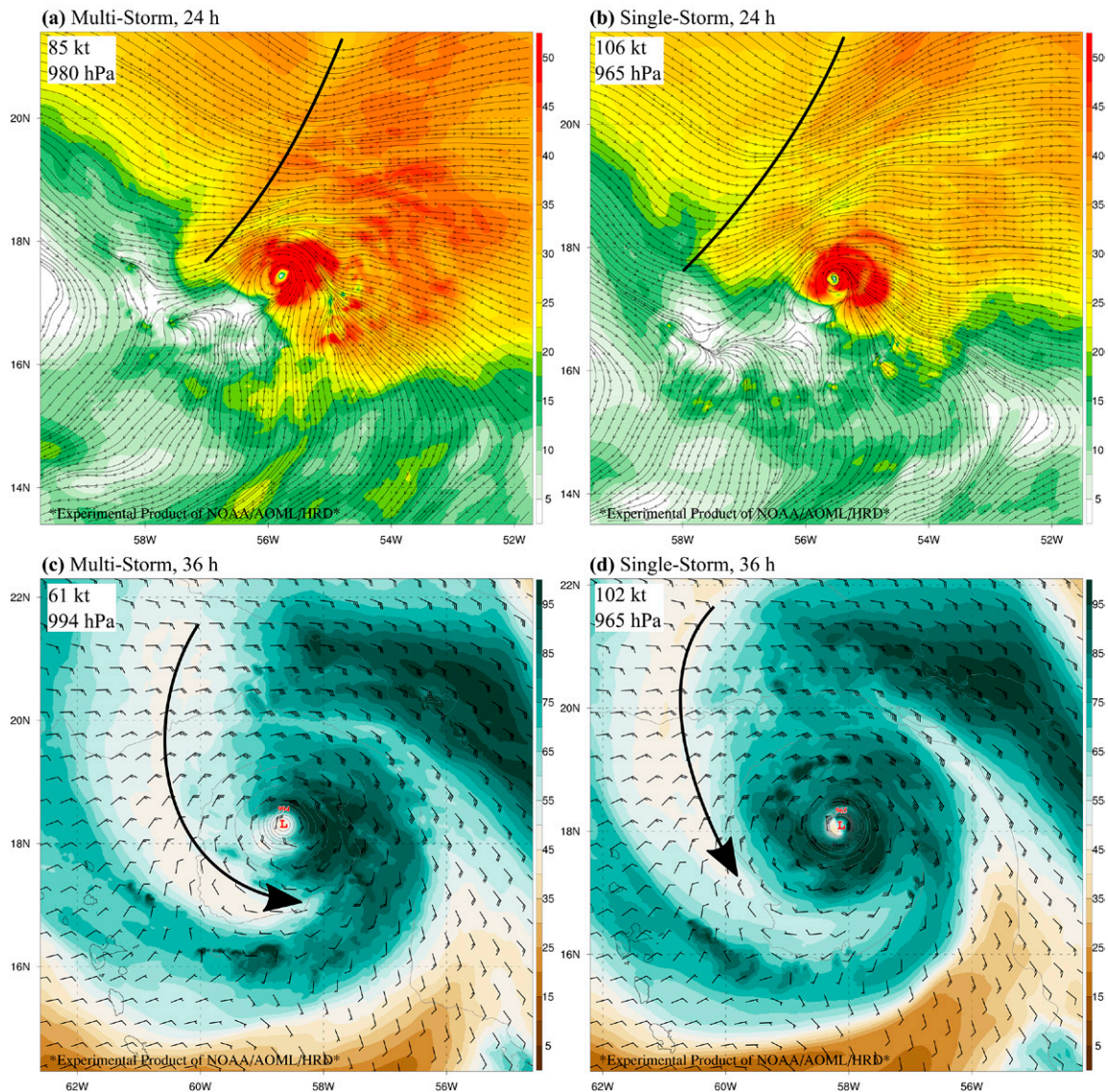
Fig. 11. The following is shown for an 8° × 8° box centered on the surface center of Jerry from forecasts initialized at 0000 UTC 19 Sep 2019: (a) deep-layer (i.e., 200 – 850 hPa) vertical wind shear magnitudes (kt) and streamlines at a lead time of 24 h from an HWRF-B MS forecast, (b) as in (a), but from an HWRF-B SS forecast, (c) 400–700-hPa weighted average relative humidity (%) at a lead time of 36 h from an MS forecast, and (d) as in (c), but from an SS forecast. In MS, Jerry had a maximum intensity of 85 kt and 980 hPa, and, in SS, Jerry had a maximum intensity of 106 kt and 965 hPa. In (a) and (b), the axis of the upper-tropospheric trough is shown as a thick black line. In (c) and (d), the inner edge of 50% relative humidity is marked by a black arrow.

wind shear was imposed by the tropical upper-tropospheric trough, and the trough axis was closer to Jerry at this time in MS than in SS (Figs. 11a,b). When moving nests were configured for both Humberto and Jerry (MS), deep-layer vertical wind shear (i.e., 200 – 850 hPa) was greater than 40 kt to the north and east of Jerry at a lead time of 24 h, indicative of hostile upper-tropospheric flow over the TC surface center (Fig. 11a). Conversely, without moving nests for Humberto, vertical wind shear values were less than 40 kt near Jerry (Fig. 11b). Hazelton et al. (2020) and other studies have shown that TCs can intensify when positioned along sharp, meridional vertical shear gradients (e.g., Hurricane Michael in 2018). However, the shear gradient was too sharp in MS to support further intensification.

Midtropospheric (i.e., 700–400 hPa mass-weighted average) relative humidity showed a thermodynamic pathway by which Humberto interacted with Jerry at a lead time of 36 h, with dry air clearly penetrating to the center of Jerry's circulation in MS and relative humidity

less than 50% wrapping around to the south of Jerry (Fig. 11c). On the other hand, in SS, midtropospheric relative humidity was more symmetric around Jerry's center and there were no signs of dry air intrusion into the core of the TC (Fig. 11d). Dry midtropospheric relative humidity was present in the environment near Jerry in both MS and SS. However, stronger vertical wind shear in MS likely allowed a pathway for dry air to enter the core of Jerry's circulation, consistent with previous studies (e.g., Rios-Berrios and Torn 2017). Therefore, the thermodynamic pathway for this particular indirect interaction was dependent upon the dynamic pathway. At lead times of 24 h and shorter, midtropospheric relative humidity in the TC inner core was symmetric in both MS and SS (not shown). Between lead times of 24 and 36 h, Jerry weakened by 24 kt and 14 hPa in MS (see Fig. 9a), while the storm was in nearly steady state in SS.

The impact of these dynamic and thermodynamic effects on Jerry is easily observed in radar reflectivity fields and vortex tilt (Fig. 12). In MS, the reflectivity had an asymmetric
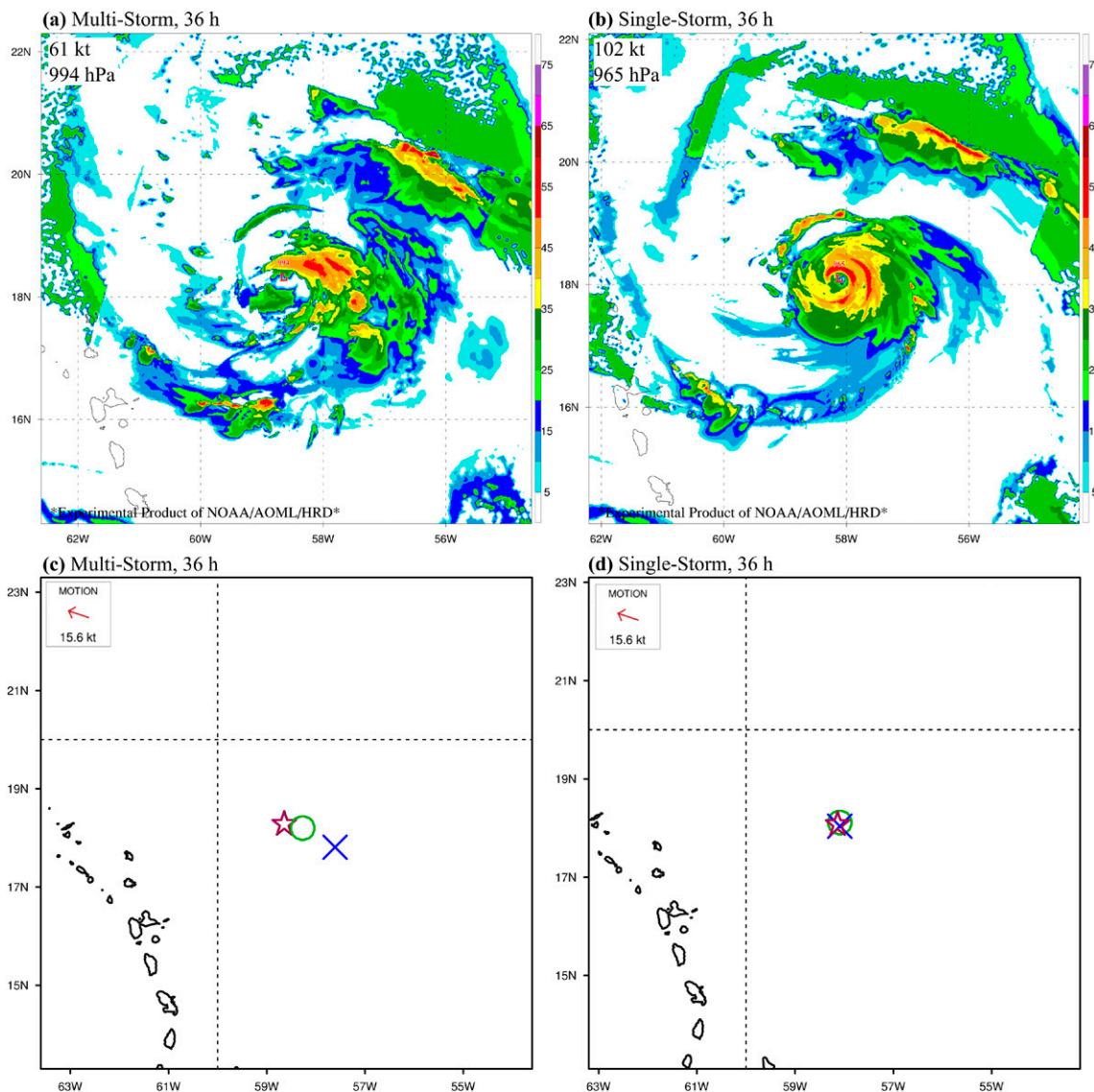
Fig. 12. The following is shown centered on the surface center of Jerry at a lead time of 36 h into forecasts initialized at 0000 UTC 19 Sep 2019: (a) simulated composite radar reflectivity (dB*Z*) from an HWRF-B MS forecast, (b) as in (a), but from an HWRF-B SS forecast, (c) vortex center locations shown at the surface (star), 500 hPa (circle), and 200 hPa ("X") from an MS forecast, along with the TC motion vector (upper left), and (d) as in (c), but from an SS forecast. Note that artifacts in simulated reflectivity in (a) and (b) are the result of postprocessing and do not impact prognostic variables in the model integration.

and ragged appearance, with almost all of the higher returns to the east (i.e., downshear) of the TC center (Fig. 12a). Reflectivity was much more symmetric in the SS forecast, with an eyewall feature and higher returns to the west of the TC center (Fig. 12b). Vortex centers at the surface, 500 hPa, and 200 hPa were used to diagnose the vortex tilt with height (Figs. 12c,d). The differences in vortex tilt between MS and SS were stark, with the vortex in the former tilting over 150 km to the east-southeast from the surface to 200 hPa and the latter showing a vertically stacked vortex throughout the depth of the troposphere. In MS, strong vertical wind shear pushed the vortex into a highly tilted structure and dry air intrusion eroded convection on the western side of the circulation.

Remote TC–TC interactions across ocean basins. The HWRF-B configurations explored in this study also shed light on how TCs interact with one another over very long distances, e.g., from one ocean basin to another. HWRF-B is well suited to study remote TC–TC interactions because of its large parent domain (see Fig. 2). Alaka et al. (2017) found that TC track forecasts improved in HWRF-B when additional TCs with moving nests were positioned more than 3,500 km away (i.e., far-field or remote TCs). In this study, the impact of far-field TCs on intensity forecasts was investigated.

In MS, TC intensity forecasts improved as the number of far-field TCs increased (Fig. 13). In other words, intensity forecasts improved when TCs were very far apart from one another at distances too great for TCs to simply communicate through interaction with the same synoptic-scale features (e.g., the tropical upper-tropospheric trough between Jerry and Humberto discussed in the previous section). Intensity forecast skill scores were consistent with the full sample when at least one and at least two remote TCs were present (cf. Figs. 13a,b with
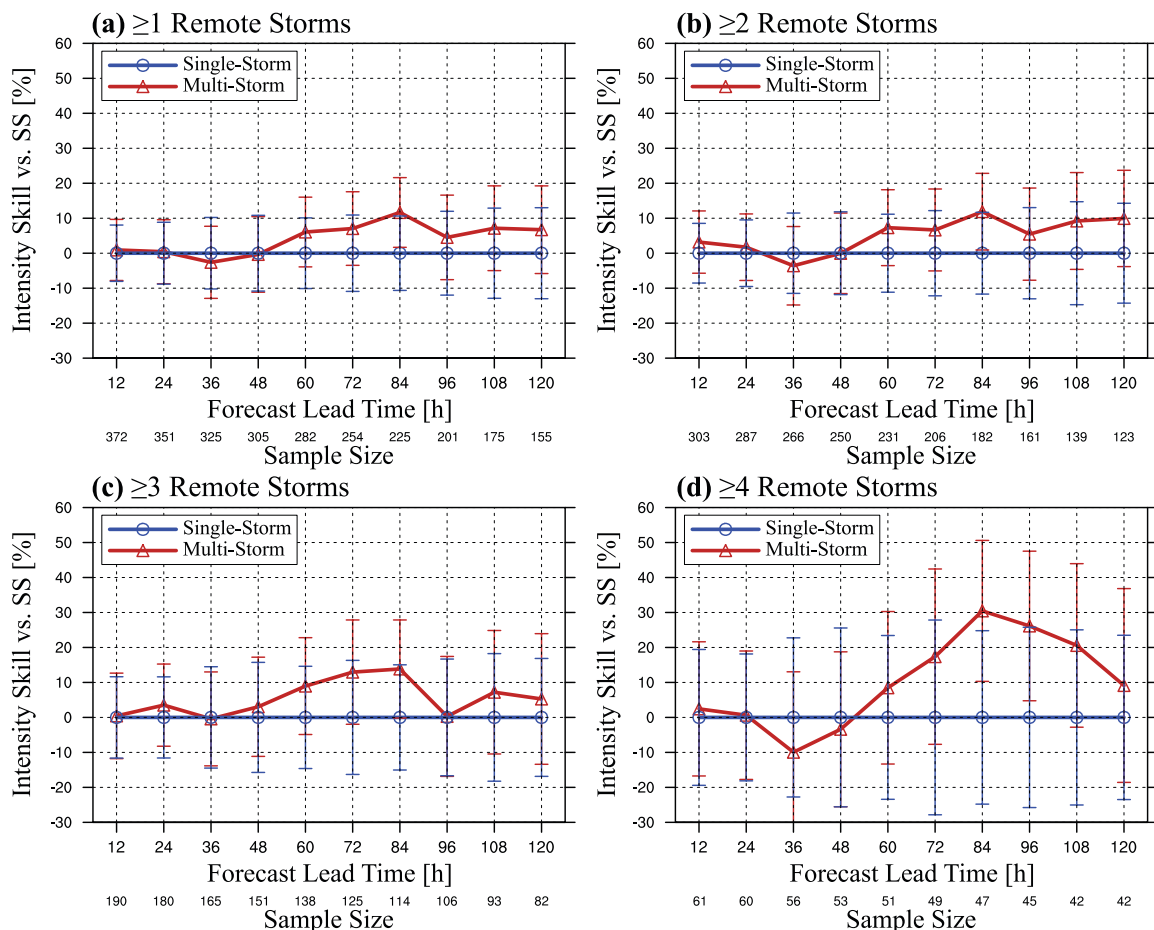

Fig. 13. As in Fig. 4c, but stratified by the number of TCs greater than 3,500 km away from the TC being verified at the model initialization time: (a) ≥1 TCs, (b) ≥2 TCs, (c) ≥3 TCs, and (d) ≥4 TCs.

Fig. 4c), likely due to the fact that a large fraction of the total sample was retained in these stratifications. When stratifying for three or more remote TCs, intensity forecast skill scores improved at many lead times, including 72 and 84 h (Fig. 13c). However, the biggest improvements were noted when the intensity forecast skill was stratified for four or more remote TCs, especially for longer lead times (Fig. 13d). In Fig. 13d, intensity forecast skill scores at 84 and 96 h were greater than 25% and were significant at the 95% confidence interval. MS track forecast skill was modestly improved (4%–8%) at lead times greater than or equal to 96 h, and was near zero at most other lead times (not shown). Track forecast skill was insignificant at every analyzed lead time. Results shown here were not sensitive to thresholds of 3,000–4,000 km. When the distance between two TCs is less than 3,000 km, they may be able to interact via modulation of the same synoptic-scale features and, thus, would be classified as indirect TC–TC interactions (see previous section).

The communication in these remote interactions was investigated in the large-scale upper troposphere for MS and SS forecasts initialized at 1200 UTC 15 September 2019, when only two TCs were active: Humberto (09L) and Kiko (13E). Humberto was an intensifying tropical storm that was moving slowly to the northeast in the western North Atlantic near the U.S. southeastern coast (Stewart 2020), while Kiko was a major hurricane that was moving almost due west in the open North Pacific Ocean (Zelinsky 2020). The MS configuration had high-resolution moving nests for both Humberto and Kiko, while the SS configuration had nests for Humberto and resolved Kiko only in the relatively coarse parent domain. Another SS forecast that had nests for Kiko and not for Humberto produced consistent results and, therefore, the discussion focuses on only one SS forecast.

The results show that Kiko and Humberto communicated via upper-tropospheric waves that emanated from each circulation starting at the model initialization time (Fig. 14). By 3 h into the MS/SS forecasts, geopotential height differences revealed waves with amplitudes up to 1 dam and wavelengths of 250–500 km. These waves had a phase speed of ~310 m s^{-1}, consistent with the shallow water gravity wave speed ($c_p = \sqrt{gH}$ = 313 m s^{-1}), where g is gravitational acceleration (9.8 m s^{-2}) and H is the scale height of the tropical troposphere (10,000 m). Although these waves had relatively low amplitude, they allowed TCs to modulate mass and momentum fields quickly over long distances.

A key question is whether or not these upper-tropospheric waves are artifacts of the high-resolution nest initialization. Gravity waves have been shown in previous studies to emanate from TCs in the upper troposphere in observations and numerical experiments,
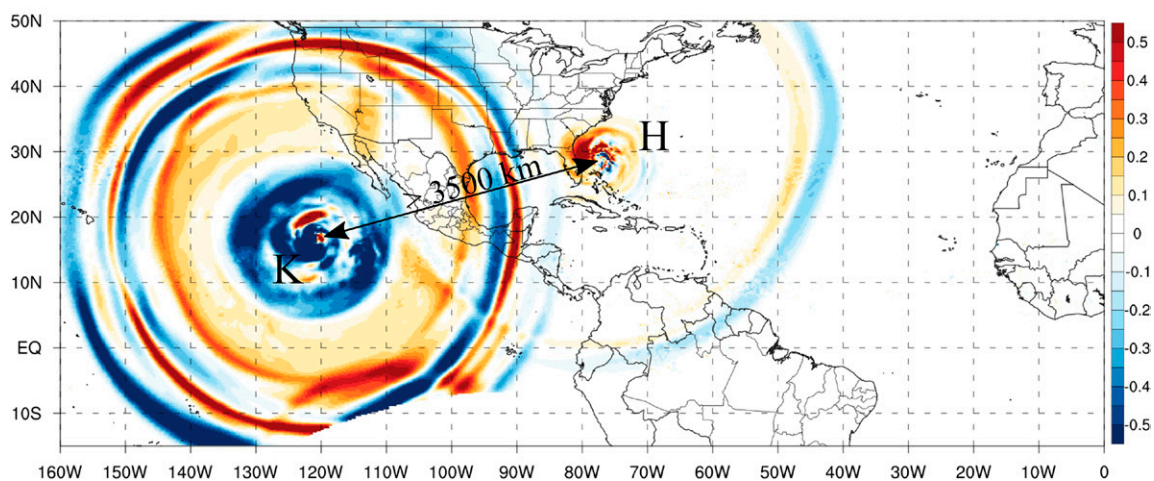

Fig. 14. Differences in 200-hPa geopotential height (dam) are shown for HWRF-B MS minus HWRF-B SS at a lead time of 3 h from forecasts initialized at 1200 UTC 15 Sep 2019. SS had high-resolution moving nests for Humberto ("H") only, while MS had high-resolution moving nests for Humberto and Kiko ("K").

and they are able to travel large distances over a relatively short period of time (e.g., Kim et al. 2009; Nolan and Zhang 2017; Molinari et al. 2019; Wang et al. 2019). However, at least at short lead times, these waves appear to be an artificial response to TC vortex initialization and modification in HWRF (see sections 4–7 in Biswas et al. 2018). These artificial waves may play a role in rebalancing the high-resolution TC initialization within the moving nest with its adjacent synoptic-scale environment. This rebalancing hypothesis is consistent with negative intensity forecast skill scores at short lead times from MS forecasts when several far-field TCs were active with moving nests (–10% at 36 h in Fig. 13d). These waves were also observed at longer lead times (not shown) with smaller amplitudes (<1 dam), supporting the notion that they were at least partially forced by deep convection associated with each TC. Remote TC–TC interactions will be the subject of a future study that will aim to identify the origin and authenticity of these upper-tropospheric waves at short and long forecast lead times.

The future of moving nests

"High-definition," storm-following nested grids (i.e., moving nests) are a cost-effective NWP model configuration option that can be used to achieve cloud-permitting resolutions in a limited area where it matters most. These nests have the capability to bridge the gap until computing resources can support uniform cloud-permitting or cloud-resolving grids in operational global models, something that will not be possible for several years. Moving nests have been a critical component of the HWRF modeling system since its development in the late 2000s, allowing for the improved simulation of clouds, convection, and sharp gradients of momentum and moisture in the eyewall and rainbands of a TC. Large increases in intensity forecast skill scores from the operational HWRF were associated with moving nest upgrades, including increasing the number of moving nests per TC from one to two and improving the resolution.

The HWRF-B system expanded the moving nest technology from a storm-centric approach to a multistorm approach. For the first time, the impact of the number of moving nests was isolated in a controlled experiment comparing multistorm and single-storm configurations of the HWRF-B system. In this experiment, intensity forecasts improved straightforwardly by adding moving nests for more TCs per forecast. Specifically, the multistorm configuration showed the largest gains at longer forecast lead times, an unsurprising result because differences in TC–TC interactions, based on the presence of moving nests, are initially small and grow with time. Improvements were also observed in statistics of intensity change. Forecast improvements in the multistorm configuration of HWRF-B were also found for three different types of TC–TC interactions: direct, indirect, and remote. The multistorm configuration simulated more realistic direct TC–TC interactions (i.e., TCs < 1,500 km apart), in particular the size of two TCs engaged in close proximity and the corresponding degree of rotation. In addition, the multistorm configuration is well suited to improve intensity forecasts for indirect TC–TC interactions (i.e., TCs 1,500–3,000 km apart), in which one TC modulates the synoptic-scale flow that then impacts a different TC. Indirect interactions were shown to occur through dynamic and thermodynamic pathways. Finally, the multistorm configuration was associated with better intensity forecasts for remote TC–TC interactions (i.e., TCs > 3,500 km apart), in which TCs communicate over long distances via upper-tropospheric waves. Remote TC–TC interactions are still not well understood and are the focus of ongoing evaluations.

The authors of this study will work with partners throughout NOAA to provide a roadmap for developments in HAFS, NOAA's next-generation hurricane research and forecast system. NOAA will support high-resolution moving nests in HAFS to optimize usage of available operational high-performance computing resources. In HAFS, this MS framework will first be implemented in a limited area domain, including synchronized two-way feedback to capture

vortex-to-regional scales and multiscale interactions. As available computing resources increase, the goal will be to implement the MS framework in a global domain to extend two-way feedback to vortex-to-global scales. The improvement of existing and development of new scale-aware physics parameterizations will also be a focus of moving nest developments in HAFS, including subgrid-scale turbulence parameterization and explicitly resolved physics using artificial intelligence technology. Data assimilation will be advanced to produce optimal initial states for outermost and moving nest domains in HAFS, including non-Gaussian all-sky satellite and scale-aware methods. The atmospheric component of HAFS will be coupled to additional Earth system model components, including the sixth version of the Modular Ocean Model (MOM6) and an advanced wave model, called WAVEWATCH III (WW3). All model components will be coupled through the Community Mediator for Earth Prediction System (CMEPS), available in UFS.

The results shown in this study should be used to improve the moving nest technology currently being developed for HAFS. For example, moving nests had the biggest positive impact on intensity forecasts in HWRF-B when configured for five TCs (Figs. 5, 13), suggesting that it would be prudent to include as many moving nests as computing resources will allow in HAFS. Furthermore, the initialization of moving nests in HAFS must be evaluated in detail to address potential issues observed in HWRF-B, including imbalances with the environment adjacent to the nests and overlapping nests. HAFS will provide an opportunity to further improve the moving nest technology that has proved to be critical for improving TC track, intensity, and structure forecasts. We will be embarking on an exciting adventure when HAFS comes online as the next-generation operational TC model at NOAA within the next few years.

Data availability statement. The numerical model simulations upon which this study is based are too large to be publicly archived with available resources. Output from the model simulations is available upon request to Dr. Ghassan J. Alaka, Jr. at NOAA/AOML/HRD (ghassan.alaka@noaa.gov). In addition, HWRF is a community model with a code repository that is publicly available at https://dtcenter.org/community-code/hurricane-wrf-hwrf/download. The HWRF-B code repository is located at https://svn-dtc-hwrf.cgd.ucar.edu/branches/HB20 and can be shared with interested parties upon request along with all information required to replicate the simulations.

References

Aberson, S. D., 2011: The impact of dropwindsonde data from the THORPEX Pacific Area Regional Campaign and the NOAA hurricane field program on tropical cyclone forecasts in the Global Forecast System. *Mon. Wea. Rev.*, **139**, 2689–2703, https://doi.org/10.1175/2011MWR3634.1.

——, and M. DeMaria, 1994: Verification of a nested barotropic hurricane track forecast model (VICBAR). *Mon. Wea. Rev.*, **122**, 2804–2815, https://doi.org/10.1175/1520-0493(1994)122<2804:VOANBH>2.0.CO;2.

Alaka, G. J., Jr., X. Zhang, S. G. Gopalakrishnan, S. B. Goldenberg, and F. D. Marks, 2017: Performance of basin-scale HWRF tropical cyclone track forecasts. *Wea. Forecasting*, **32**, 1253–1271, https://doi.org/10.1175/WAF-D-16-0150.1.

——, Z. Zhang, F. D. Marks, and R. Atlas, 2019: Track uncertainty in high-resolution HWRF ensemble forecasts of Hurricane Joaquin. *Wea. Forecasting*, **34**, 1889–1908, https://doi.org/10.1175/WAF-D-19-0028.1.

——, D. Sheinin, B. Thomas, L. Gramer, Z. Zhang, B. Liu, H.-S. Kim, and A. Mehra, 2020: A hydrodynamical atmosphere/ocean coupled modeling system for multiple tropical cyclones. *Atmosphere*, **11**, 869, https://doi.org/10.3390/atmos11080869.

Archambault, H. M., L. F. Bosart, D. Keyser, and J. M. Cordeira, 2013: A climatological analysis of the extratropical flow response to recurving western North Pacific tropical cyclones. *Mon. Wea. Rev.*, **141**, 2325–2346, https://doi.org/10.1175/MWR-D-12-00257.1.

——, D. Keyser, L. F. Bosart, C. A. Davis, and J. M. Cordeira, 2015: A composite perspective of the extratropical flow response to recurving western North Pacific tropical cyclones. *Mon. Wea. Rev.*, **143**, 1122–1141, https://doi.org/10.1175/MWR-D-14-00270.1.

Atlas, R., V. Tallapragada, and S. G. Gopalakrishnan, 2015: Advances in tropical cyclone intensity forecasts. *Mar. Technol. J.*, **49**, 149–160, https://doi.org/10.4031/MTSJ.49.6.2.

Avila, L. A., 2019: Hurricane Lorena (EP152019). National Hurricane Center Tropical Cyclone Rep., 20 pp., www.nhc.noaa.gov/data/tcr/EP152019_Lorena.pdf.

Bao, J.-W., S. G. Gopalakrishnan, S. A. Michelson, F. D. Marks, and M. T. Montgomery, 2012: Impact of physics representations in the HWRFX on simulated hurricane structure and pressure–wind relationships. *Mon. Wea. Rev.*, **140**, 3278–3299, https://doi.org/10.1175/MWR-D-11-00332.1.

Bender, M. A., I. Ginis, R. Tuleya, B. Thomas, and T. Marchok, 2007: The operational GFDL coupled hurricane–ocean prediction system and a summary of its performance. *Mon. Wea. Rev.*, **135**, 3965–3989, https://doi.org/10.1175/2007MWR2032.1.

Berg, R. J., 2019: Tropical Storm Mario (EP142019). National Hurricane Center Tropical Cyclone Rep., 14 pp., www.nhc.noaa.gov/data/tcr/EP142019_Mario.pdf.

Biswas, M. K., L. Carson, K. Newman, D. Stark, E. Kalina, E. Grell, and J. Frimel, 2018: Community HWRF users' guide V4.0a. NCAR Tech. Note, 162 pp., https://dtcenter.org/sites/default/files/community-code/hwrf/docs/users_guide/HWRF-UG-2018.pdf.

Brand, S., 1970: Interaction of binary cyclones of the western North Pacific Ocean. *J. Appl. Meteor.*, **9**, 433–441, https://doi.org/10.1175/1520-0450(1970)009<0433:IOBTCO>2.0.CO;2.

Brown, D. P., 2019: Hurricane Jerry (AL102019). National Hurricane Center Tropical Cyclone Rep., 17 pp., www.nhc.noaa.gov/data/tcr/AL102019_Jerry.pdf.

Cangialosi, J., S. S. Chen, and J. Michalakes, 2005: Hurricane simulations using a vortex-following nested grid in MM5 and WRF. *WRF/MM5 Users' Workshop*, Boulder, CO, NCAR.

Carr, L. E., R. L. Elsberry, and M. A. Booth, 1999: Condensed and updated version of the systematic approach meteorological knowledge base western North Pacific. Naval Postgraduate School Rep. NPS-MR-00-001, 140 pp., https://hdl.handle.net/10945/28702.

Davis, C., and Coauthors, 2008: Prediction of landfalling hurricanes with the Advanced Hurricane WRF Model. *Mon. Wea. Rev.*, **136**, 1990–2005, https://doi.org/10.1175/2007MWR2085.1.

——, W. Wang, J. Dudhia, and R. Torn, 2010: Does increased horizontal resolution improve hurricane wind forecasts? *Wea. Forecasting*, **25**, 1826–1841, https://doi.org/10.1175/2010WAF2222423.1.

Dong, J., and Coauthors, 2020: Hurricane Analysis and Forecast System (HAFS) Stand-Alone Regional Model (SAR) 2019 Atlantic hurricane season real-time forecasts. *100th Annual Meeting*, Boston, MA, Amer. Meteor. Soc., 368586, https://ams.confex.com/ams/2020Annual/webprogram/Paper368586.html.

Dong, K., and C. J. Neumann, 1983: On the relative motion of binary tropical cyclones. *Mon. Wea. Rev.*, **111**, 945–953, https://doi.org/10.1175/1520-0493(1983)111<0945:OTRMOB>2.0.CO;2.

Doyle, J. D., and Coauthors, 2014: Tropical cyclone prediction using COAMPS-TC. *Oceanography*, **27** (3), 104–115, https://doi.org/10.5670/oceanog.2014.72.

Dudhia, J., and Coauthors, 2008: Prediction of Atlantic tropical cyclones with the Advanced Hurricane WRF (AHW) Model. *28th Conf. on Hurricanes and Tropical Meteorology*, Orlando, FL, Amer. Meteor. Soc., 18A.2, https://ams.confex.com/ams/pdfpapers/138004.pdf.

Fierro, A. O., R. F. Rogers, F. D. Marks, and D. S. Nolan, 2009: The impact of horizontal grid spacing on the microphysical and kinematic structures of strong tropical cyclones simulated with the WRF-ARW Model. *Mon. Wea. Rev.*, **137**, 3717–3743, https://doi.org/10.1175/2009MWR2946.1.

Fujiwhara, S., 1921: The mutual tendency towards symmetry of motion and its application as a principle in meteorology. *Quart. J. Roy. Meteor. Soc.*, **47**, 287–292, https://doi.org/10.1002/qj.49704720010.

Gall, R., J. Franklin, F. Marks, E. N. Rappaport, and F. Toepfer, 2013: The Hurricane Forecast Improvement Project. *Bull. Amer. Meteor. Soc.*, **94**, 329–343, https://doi.org/10.1175/BAMS-D-12-00071.1.

Gao, K., J.-H. Chen, L. Harris, Y. Sun, and S.-J. Lin, 2019: Skillful prediction of monthly major hurricane activity in the North Atlantic with two-way nesting. *Geophys. Res. Lett.*, **46**, 9222–9230, https://doi.org/10.1029/2019GL083526.

Goldenberg, S. B., S. G. Gopalakrishnan, T. Quirino, F. D. Marks Jr., V. Tallapragada, S. Trahan, X. Zhang, and R. Atlas, 2015: The 2012 triply nested, high-resolution operational version of the Hurricane Weather Research and Forecasting System (HWRF): Track and intensity forecast verifications. *Wea. Forecasting*, **30**, 710–729, https://doi.org/10.1175/WAF-D-14-00098.1.

Gopalakrishnan, S. G., N. Surgi, R. Tuleya, and Z. Janjic, 2006: NCEP's two-way-interactive-moving-nest NMM-WRF modeling system for hurricane forecasting. *27th Conf. on Hurricanes and Tropical Meteorology*, Monterey, CA, Amer. Meteor. Soc., 7A.3, https://ams.confex.com/ams/pdfpapers/107899.pdf.

——, F. D. Marks, X. Zhang, J.-W. Bao, K.-S. Yeh, and R. Atlas, 2011: The experimental HWRF system: A study on the influence of horizontal resolution on the structure and intensity changes in tropical cyclones using an idealized framework. *Mon. Wea. Rev.*, **139**, 1762–1784, https://doi.org/10.1175/2010MWR3535.1.

——, S. B. Goldenberg, T. S. Quirino, X. Zhang, F. D. Marks, K.-S. Yeh, R. Atlas, and V. Tallapragada, 2012: Toward improving high-resolution numerical hurricane forecasting: Influence of model horizontal grid resolution, initialization, and physics. *Wea. Forecasting*, **27**, 647–666, https://doi.org/10.1175/WAF-D-11-00055.1.

——, F. D. Marks, J. A. Zhang, X. Zhang, J.-W. Bao, and V. Tallapragada, 2013: A study of the impacts of vertical diffusion on the structure and intensity of the tropical cyclones using the high resolution HWRF system. *J. Atmos. Sci.*, **70**, 524–541, https://doi.org/10.1175/JAS-D-11-0340.1.

——, and Coauthors, 2020: 2019 HFIP R&D activities summary: Recent results and operational implementation. NOAA HFIP Tech. Rep. HFIP2020-1, 42 pp., https://hfip.org/sites/default/files/documents/hfip-annualreport-fy2019.pdf.

Grell, G. A., J. Dudhia, and D. R. Stauffer, 1995: A description of the fifth-generation Penn State/NCAR mesoscale model (MM5). NCAR Tech. Note NCAR/TN-398+STR, 122 pp.

Harris, L., and S.-J. Lin, 2013: A two-way nested global-regional dynamical core on the cubed-sphere grid. *Mon. Wea. Rev.*, **141**, 283–306, https://doi.org/10.1175/MWR-D-11-00201.1.

Harrison, E. J., Jr., 1973: Three-dimensional numerical simulations of tropical systems using nested finite grids. *J. Atmos. Sci.*, **30**, 1528–1543, https://doi.org/10.1175/1520-0469(1973)030<1528:TDNSOT>2.0.CO;2.

——, and R. L. Elsberry, 1972: A method for incorporating nested finite grids in the solution of systems of geophysical equations. *J. Atmos. Sci.*, **29**, 1235–1245, https://doi.org/10.1175/1520-0469(1972)029<1235:AMFINF>2.0.CO;2.

Hazelton, A., X. Zhang, S. Gopalakrishnan, W. Ramstrom, F. Marks, and J. A. Zhang, 2020: High-resolution ensemble HFV3 forecasts of Hurricane Michael (2018): Rapid intensification in shear. *Mon. Wea. Rev.*, **148**, 2009–2032, https://doi.org/10.1175/MWR-D-19-0275.1.

——, and Coauthors, 2021: 2019 Atlantic hurricane forecasts from the global-nested Hurricane Analysis and Forecast System: Composite statistics and key events. *Wea. Forecasting*, **36**, 519–538, https://doi.org/10.1175/WAF-D-20-0044.1.

——, and Coauthors, 2022: Performance of 2020 real-time Atlantic hurricane forecasts from high-resolution global-nested hurricane models: HAFS-globalnest and GFDL T-SHiELD. *Wea. Forecasting*, **37**, 143–161, https://doi.org/10.1175/WAF-D-21-0102.1.

Hill, G., 1968: Grid telescoping in numerical weather prediction. *J. Appl. Meteor.*, **7**, 29–38, https://doi.org/10.1175/1520-0450(1968)007<0029:GTINWP>2.0.CO;2.

Homeyer, C. R., and K. P. Bowman, 2013: Rossby wave breaking and transport between the tropics and extratropics above the subtropical jet. *J. Atmos. Sci.*, **70**, 607–626, https://doi.org/10.1175/JAS-D-12-0198.1.

Janjić, Z. I., J. P. Gerrity Jr., and S. Nickovic, 2001: An alternative approach to nonhydrostatic modeling. *Mon. Wea. Rev.*, **129**, 1164–1178, https://doi.org/10.1175/1520-0493(2001)129<1164:AAATNM>2.0.CO;2.

Jones, R. W., 1977: A nested grid for a three-dimensional model of a tropical cyclone. *J. Atmos. Sci.*, **34**, 1528–1553, https://doi.org/10.1175/1520-0469(1977)034<1528:ANGFAT>2.0.CO;2.

Kim, S.-Y., H.-Y. Chun, and D. L. Wu, 2009: A study on stratospheric gravity waves generated by Typhoon Ewiniar: Numerical simulations and satellite observations. *J. Geophys. Res.*, **114**, D22104, https://doi.org/10.1029/2009JD011971.

Kurihara, Y., and M. A. Bender, 1980: Use of a movable nested-mesh model for tracking a small vortex. *Mon. Wea. Rev.*, **108**, 1792–1809, https://doi.org/10.1175/1520-0493(1980)108<1792:UOAMNM>2.0.CO;2.

——, G. J. Tripoli, and M. A. Bender, 1979: Design of a movable nested-mesh primitive equation model. *Mon. Wea. Rev.*, **107**, 239–249, https://doi.org/10.1175/1520-0493(1979)107<0239:DOAMNM>2.0.CO;2.

——, R. E. Tuleya, and M. A. Bender, 1998: The GFDL Hurricane Prediction System and its performance in the 1995 hurricane season. *Mon. Wea. Rev.*, **126**, 1306–1322, https://doi.org/10.1175/1520-0493(1998)126<1306:TGHPSA>2.0.CO;2.

Kwon, H. J., S. H. Won, M. H. Ahn, A. S. Suh, and H. S. Chung, 2002: MM5 typhoon simulation using autonomous moving nest. *Third US–Korea Joint Workshop on Storm and Mesoscale Weather Analysis and Prediction*, Boulder, CO, UCAR, http://danida.vnu.edu.vn/cpis/files/Refs/TCs/MM5%20typhoon%20simulation%20using%20autonomous%20moving%20nest.pdf.

Lander, M., and G. J. Holland, 1993: On the interaction of tropical-cyclone-scale vortices. I: Observations. *Quart. J. Roy. Meteor. Soc.*, **119**, 1347–1361, https://doi.org/10.1002/qj.49711951406.

Ley, G. W., and R. L. Elsberry, 1976: Forecasts of Typhoon Irma using a nested-grid model. *Mon. Wea. Rev.*, **104**, 1154–1161, https://doi.org/10.1175/1520-0493(1976)104<1154:FOTIUA>2.0.CO;2.

Lin, N., J. A. Smith, G. Villarini, T. P. Marchok, and M. L. Baeck, 2010: Modeling extreme rainfall, winds, and surge from Hurricane Isabel (2003). *Wea. Forecasting*, **25**, 1342–1361, https://doi.org/10.1175/2010WAF2222349.1.

Lin, S.-J., 2004: A "vertically Lagrangian" finite-volume dynamical core for global models. *Mon. Wea. Rev.*, **132**, 2293–2307, https://doi.org/10.1175/1520-0493(2004)132<2293:AVLFDC>2.0.CO;2.

——, and R. B. Rood, 1996: Multidimensional flux-form semi-Lagrangian transport schemes. *Mon. Wea. Rev.*, **124**, 2046–2070, https://doi.org/10.1175/1520-0493(1996)124<2046:MFFSLT>2.0.CO;2.

Liu, Y., D.-L. Zhang, and M. K. Yau, 1997: A multiscale numerical study of Hurricane Andrew (1992). Part I: Explicit simulation and verification. *Mon. Wea. Rev.*, **125**, 3073–3093, https://doi.org/10.1175/1520-0493(1997)125<3073:AMNSOH>2.0.CO;2.

Marks, F., and Coauthors, 1998: Landfalling tropical cyclones: Forecast problems and associated research opportunities. *Bull. Amer. Meteor. Soc.*, **79**, 305–323, https://doi.org/10.1175/1520-0477(1998)079<0285:QPFROT>2.0.CO;2.

Mathur, N. B., 1974: A multiple-grid primitive equation model to simulate the development of an asymmetric hurricane (Isbell, 1964). *J. Atmos. Sci.*, **31**, 371–393, https://doi.org/10.1175/1520-0469(1974)031<0371:AMGPEM>2.0.CO;2.

Mehra, A., V. Tallapragada, Z. Zhang, B. Liu, L. Zhu, W. Wang, and H.-S. Kim, 2018: Advancing the state of the art in operational tropical cyclone forecasting at NCEP. *Trop. Cyclone Res. Rev.*, **7**, 51–56, https://doi.org/10.6057/2018TCRR01.06.

Michalakes, J., J. Dudhia, D. Gill, T. Henderson, J. Klemp, W. Skamarock, and W. Wang, 2005: The Weather Research and Forecast Model: Software architecture and performance. *Use of High Performance Computing in Meteorology*, W. Zwieflhofer and G. Mozdzynski, Eds., World Scientific, 156–168, https://doi.org/10.1142/9789812701831_0012.

Molinari, J., M. Rosenmayer, D. Vollaro, and S. D. Ditchek, 2019: Turbulence variations in the upper troposphere in tropical cyclones from NOAA G-IV flight-level vertical acceleration data. *J. Appl. Meteor. Climatol.*, **58**, 569–583, https://doi.org/10.1175/JAMC-D-18-0148.1.

National Weather Service, 2017: Governance model for Unified Forecast System for NCEP's Production Suite. National Weather Service Doc., 14 pp., www.weather.gov/media/sti/nggps/Presentations%202017/Implementation/SIP%20Governance%20Model_%20Public_%20Version%201.pdf.

Nolan, D. S., and J. A. Zhang, 2017: Spiral gravity waves radiating from tropical cyclones. *Geophys. Res. Lett.*, **44**, 3924–3931, https://doi.org/10.1002/2017GL073572.

Ookochi, Y., 1974: Numerical prediction of typhoon movements with use of the multiple grid nesting. *J. Meteor. Soc. Japan*, **52**, 387–390, https://doi.org/10.2151/jmsj1965.52.4_387.

Papin, P. P., L. F. Bosart, and R. D. Torn, 2020: A feature-based approach to classifying summertime potential vorticity streamers linked to Rossby wave breaking in the North Atlantic basin. *J. Climate*, **33**, 5953–5969, https://doi.org/10.1175/JCLI-D-19-0812.1.

Phillips, N. A., and J. Shukla, 1973: On the strategy of combining coarse and fine grid meshes in numerical weather prediction. *J. Appl. Meteor.*, **12**, 763–770, https://doi.org/10.1175/1520-0450(1973)012<0763:OTSOCC>2.0.CO;2.

Rappaport, E. N., and Coauthors, 2009: Advances and challenges at the National Hurricane Center. *Wea. Forecasting*, **24**, 395–419, https://doi.org/10.1175/2008WAF2222128.1.

Rios-Berrios, R., and R. D. Torn, 2017: Climatological analysis of tropical cyclone intensity changes under moderate vertical wind shear. *Mon. Wea. Rev.*, **145**, 1717–1738, https://doi.org/10.1175/MWR-D-16-0350.1.

Rood, R. B., and Coauthors, 2018: Organizing research to operations transition. NOAA UFS Tech. Rep., 36 pp., https://ufscommunity.org/wp-content/uploads/2019/10/20181130_Organizing_Research_to_Operations_Transition.pdf.

Rotunno, R., Y. Chen, W. Wang, C. Davis, J. Dudhia, and G. J. Holland, 2009: Large-eddy simulation of an idealized tropical cyclone. *Bull. Amer. Meteor. Soc.*, **90**, 1783–1788, https://doi.org/10.1175/2009BAMS2884.1.

Skamarock, W. C., and J. B. Klemp, 2008: A time-split nonhydrostatic atmospheric model for weather research and forecasting applications. *J. Comput. Phys.*, **227**, 3465–3485, https://doi.org/10.1016/j.jcp.2007.01.037.

Stewart, S. R., 2020: Hurricane Humberto (AL092019). National Hurricane Center Tropical Cyclone Rep., 44 pp., www.nhc.noaa.gov/data/tcr/AL092019_Humberto.pdf.

Susca-Lopata, G., J. Zawislak, E. J. Zipser, and R. F. Rogers, 2015: The role of observed environmental conditions and precipitation evolution in the rapid intensification of Hurricane Earl (2010). *Mon. Wea. Rev.*, **143**, 2207–2223, https://doi.org/10.1175/MWR-D-14-00283.1.

Tallapragada, V., C. Kieu, Y. Kwon, S. Trahan, Q. Liu, Z. Zhang, and I.-H. Kwon, 2014: Evaluation of storm structure from the operational HWRF model during 2012 implementation. *Mon. Wea. Rev.*, **142**, 4308–4325, https://doi.org/10.1175/MWR-D-13-00010.1.

Wang, Y., 2001: An explicit simulation of tropical cyclones with a triply nested movable mesh primitive equation model: TCM3. Part I: Model

description and control experiment. *Mon. Wea. Rev.*, **129**, 1370–1394, https://doi.org/10.1175/1520-0493(2001)129<1370:AESOTC>2.0.CO;2.

——, L. Zhang, and Y. Zhang, 2019: Effects of tropospheric vertical wind shear on gravity waves generated by tropical cyclones. *Geophys. Res. Lett.*, **46**, 4523–4530, https://doi.org/10.1029/2019GL082085.

Wu, L., S. A. Braun, J. Halverson, and G. Heymsfield, 2006: A numerical study of Hurricane Erin (2001). Part I: Model verification and storm evolution. *J. Atmos. Sci.*, **63**, 65–86, https://doi.org/10.1175/JAS3597.1.

Xiao, Q., X. Zhang, C. Davis, J. Tuttle, G. Holland, and P. J. Fitzpatrick, 2009: Experiments of hurricane initialization with airborne Doppler radar data for the Advanced Research Hurricane WRF (AHW) Model. *Mon. Wea. Rev.*, **137**, 2758–2777, https://doi.org/10.1175/2009MWR2828.1.

Zelinsky, D. A., 2020: Hurricane Kiko (EP132019). National Hurricane Center Tropical Cyclone Rep., 16 pp., www.nhc.noaa.gov/data/tcr/EP132019_Kiko.pdf.

Zhang, B., R. S. Lindzen, V. Tallapragada, F. Weng, Q. Liu, J. A. Sippel, Z. Ma, and M. A. Bender, 2016: Increasing vertical resolution in US models to improve track forecasts of Hurricane Joaquin with HWRF as an example. *Proc. Natl. Acad. Sci. USA*, **113**, 11 765–11 769, https://doi.org/10.1073/pnas.1613800113.

Zhang, D.-L., H.-R. Chang, N. L. Seaman, T. T. Warner, and J. M. Fritsch, 1986: A two-way interactive nesting procedure with variable terrain resolution. *Mon. Wea. Rev.*, **114**, 1330–1339, https://doi.org/10.1175/1520-0493(1986)114<1330:ATWINP>2.0.CO;2.

Zhang, X., T. Quirino, K.-S. Yeh, S. Gopalakrishnan, F. Marks, S. Goldenberg, and S. Aberson, 2011: HWRFx: Improving hurricane forecasts with high-resolution modeling. *Comput. Sci. Eng.*, **13**, 13–21, https://doi.org/10.1109/MCSE.2010.121.

——, S. G. Gopalakrishnan, S. Trahan, T. S. Quirino, Q. Liu, Z. Zhang, G. J. Alaka, and V. Tallapragada, 2016: Representing multiple scales in the Hurricane Weather Research and Forecasting Modeling system: Design of multiple sets of movable multilevel nesting and the basin-scale HWRF forecast application. *Wea. Forecasting*, **31**, 2019–2034, https://doi.org/10.1175/WAF-D-16-0087.1.